JEM Journal of Experimental Medicine

ARTICLE

CD47 blockade enhances the efficacy of intratumoral STING-targeting therapy by activating phagocytes

Akemi Kosaka[1*], Kei Ishibashi[1,2*], Toshihiro Nagato[1], Hidemitsu Kitamura[3], Yukio Fujiwara[4], Syunsuke Yasuda[2], Marino Nagata[1], Shohei Harabuchi[1,5], Ryusuke Hayashi[1,5], Yuki Yajima[1], Kenzo Ohara[5], Takumi Kumai[5], Naoko Aoki[1], Yoshihiro Komohara[4], Kensuke Oikawa[1], Yasuaki Harabuchi[5], Masahiro Kitada[2], Hiroya Kobayashi[1], and Takayuki Ohkuri[1*]

Activation of STING signaling plays an important role in anti-tumor immunity, and we previously reported the anti-tumor effects of STING through accumulation of M1-like macrophages in tumor tissue treated with a STING agonist. However, myeloid cells express SIRPα, an inhibitory receptor for phagocytosis, and its receptor, CD47, is overexpressed in various cancer types. Based on our findings that breast cancer patients with highly expressed CD47 have poor survival, we evaluated the therapeutic efficacy and underlying mechanisms of combination therapy with the STING ligand cGAMP and an antagonistic anti-CD47 mAb using E0771 mouse breast cancer cells. Anti-CD47 mAb monotherapy did not suppress tumor growth in our setting, whereas cGAMP and anti-CD47 mAb combination therapy inhibited tumor growth. The combination therapy enhanced phagocytosis of tumor cells and induced systemic anti-tumor immune responses, which rely on STING and type I IFN signaling. Taken together, our findings indicate that coadministration of cGAMP and an antagonistic anti-CD47 mAb may be promising for effective cancer immunotherapy.

Introduction

CD47 is expressed on the surface of almost all cells and inhibits phagocytosis by monocytes/macrophages through binding to its receptor, signal regulatory protein α (SIRPα), which is a monocyte/macrophage immune checkpoint molecule with inhibitory function (Okazawa et al., 2005; Oldenborg et al., 2000; Vernon-Wilson et al., 2000). CD47 is also expressed in many tumor types, including ovarian, breast, colon, and prostate cancers; glioblastoma multiforme; and hepatocellular carcinoma (Willingham et al., 2012). In addition, increased CD47 mRNA expression levels were correlated with poor clinical outcomes in patients with ovarian cancer, gliomas, glioblastomas, acute myeloid leukemia, non-Hodgkin's lymphoma, and hepatocellular carcinoma (Chao et al., 2010; Chen et al., 2019; Majeti et al., 2009). Therefore, blocking CD47-SIRPα signaling with an antagonistic mAb is a rational strategy, and several clinical trials of antagonistic mAbs are currently underway (Murata et al., 2018).

Stimulator of interferon genes (STING) is one of the important adaptors for cytosolic DNA sensing, and it plays a critical role in host defense against viral and intracellular bacterial infections by inducing type I IFN signaling (Fuertes et al., 2013; Gajewski et al., 2013; Ishikawa et al., 2009). In addition, we have previously demonstrated that STING spontaneously contributes to anti-tumor immune responses via type I IFN signaling in the tumor microenvironment (Ohkuri et al., 2014). Other groups have reported that activation of the STING signaling pathway leads to the induction of anti-tumor immunity through various mechanisms (Marcus et al., 2018; Takashima et al., 2016; Watkins-Schulz et al., 2019). Furthermore, we recently found that $CD11b^+Ly6C^+F4/80^+$ monocytes/macrophages were transiently accumulated in the tumor site by intratumoral injection of the STING ligand cyclic GMP-AMP (cGAMP). The migrating monocytes/macrophages showed phagocytic activity and high expression levels of genes that promote anti-tumor immunity, suggesting that these cells are classically activated M1-like macrophages (Ohkuri et al., 2017). We therefore hypothesized that intratumoral injection of a STING ligand would be suitable for combination therapy regimens using monocyte/macrophage-modulating drugs, such as an antagonistic anti-CD47 mAb, to promote phagocytosis by the accumulated monocytes/macrophages in the tumor microenvironment.

[1]Department of Pathology, Asahikawa Medical University, Asahikawa, Japan; [2]Respiratory and Breast Center, Asahikawa Medical University Hospital, Asahikawa, Japan; [3]Division of Functional Immunology, Section of Disease Control, Institute for Genetic Medicine, Hokkaido University, Sapporo, Japan; [4]Department of Cell Pathology, Graduate School of Medical Sciences, Faculty of Life Sciences, Kumamoto University, Kumamoto, Japan; [5]Department of Otolaryngology, Head and Neck Surgery, Asahikawa Medical University, Asahikawa, Japan.

*A. Kosaka, K. Ishibashi, and T. Ohkuri contributed equally to this paper; Correspondence to Takayuki Ohkuri: ohkurit@asahikawa-med.ac.jp; Hiroya Kobayashi: hiroya@asahikawa-med.ac.jp.

In this study, we demonstrated that CD47 was highly expressed in 36.7% of breast cancer specimens by immunohistochemistry (IHC) analysis, and CD47 overexpression significantly reduced recurrence-free survival (RFS) and tended to predict poor overall survival (OS). In analyses using a mouse breast cancer model, intratumoral administration of cGAMP combined with an antagonistic anti-CD47 mAb enhanced anti-tumor immune responses by promoting monocyte/macrophage phagocytosis in the tumor microenvironment and tumor-specific $CD8^+$ T cell responses in the LNs. The combination therapy also induced systemic anti-tumor effects, suggesting that intratumoral coadministration of cGAMP with monocyte/macrophage-modulating drugs such as an antagonistic anti-CD47 mAb would provide an attractive therapeutic strategy.

Results

Overexpression of CD47 in tumors is associated with poor prognosis and high infiltration of $CD8^+$ and $CD68^+$ cells in breast cancer patients

To investigate whether CD47 expression correlates with prognosis in breast cancer, we evaluated CD47 expression in breast cancer tissues from 98 patients by IHC. The results of the initial evaluation were 15, 47, 25, and 11 patients who were classified as having no, weak, moderate, and strong staining, respectively. For further analysis, the patients were grouped into negative (no and weak staining) and positive (moderate and strong staining) expression specimens (62 and 36 patients, respectively; Fig. 1 A). We found that CD47 overexpression was significantly correlated with lymphatic duct invasion, vascular invasion, and HLA-G expression, but there was no correlation with other factors such as menopause status, nuclear grade, pathological stage, LN metastasis, and estrogen receptor (ER), progesterone receptor (PR), and human epidermal growth factor receptor 2 (HER2) expression levels (Table 1). Furthermore, patients with CD47 overexpression showed significantly poor RFS ($P = 0.0343$) and a similar but nonsignificant trend for decreased OS ($P = 0.0569$) compared with those with CD47-low expression (Fig. 1 B). Moreover, to address the associations between CD47 expression and immune cell migration in tumors, quantification of $CD8^+$ and $CD68^+$ cells in 91 specimens was performed (Fig. 1, C and D). There were no associations between patient survival and infiltrations of $CD8^+$ or $CD68^+$ cells (Fig. 1, E and F), although tumor infiltrations of $CD8^+$ and $CD68^+$ cells showed a positive correlation (Fig. 1 G and Table 2). Moreover, CD47 expression was positively associated with the infiltrations of $CD8^+$ and $CD68^+$ cells (Fig. 1, H and I; and Table 3), while HLA-G expression was positively associated with the infiltration of only $CD8^+$, but not $CD68^+$, cells (Fig. 1, J and K). These data suggest that CD47 may be a useful prognostic biomarker for tumor progression, and high infiltration of $CD8^+$ cells is positively associated with both CD47 and HLA-G immunosuppressive molecules in patients with breast cancer.

Intratumoral coinjection of cGAMP and anti-CD47 mAb efficiently suppresses tumor growth

Because we previously demonstrated that intratumoral administration of the STING ligand cGAMP promotes accumulation of M1-like macrophages with phagocytic activity in the tumor microenvironment (Ohkuri et al., 2017), we hypothesized that combination therapy of cGAMP and an antagonistic antibody to CD47 would enhance both phagocytosis of cancer cells at the tumor site and activation of tumor antigen-specific T cells in the draining LNs, resulting in increased anti-tumor activity in patients with CD47-overexpressing breast cancer. To evaluate this hypothesis, we first assessed the efficacy of the combination therapy using the mouse breast cancer cell line E0771, which expressed high levels of CD47. IFN-β or IFN-γ up-regulated H-$2K^b$ and programmed death-ligand 1 (PD-L1), but not CD47 (Fig. 2 A). We found a synergistic effect of intratumoral coinjection of cGAMP and anti-CD47 mAb on increased accumulation of $CD11b^+Ly6C^+$ monocytes/macrophages in tumor-infiltrating lymphocytes (TILs), although monotherapy with anti-CD47 mAb reduced the percentage of $CD11b^+Ly6C^+$ cells (Fig. 2 B). In contrast, migration of $CD11c^+$MHC-$II^+CD24^+CD11b^-CD103^+$ type 1 conventional dendritic cells (cDC1) into the tumor site was not affected by any treatment (Fig. 2 B and Fig. S1 B). The combination therapy significantly delayed tumor growth and prolonged survival compared with cGAMP or anti-CD47 mAb monotherapy (median survival time: undefined vs. 47.5 or 44 d, respectively), although cGAMP monotherapy exhibited anti-tumor activity compared with control and anti-CD47 mAb monotherapy (median survival time: 47.5 vs. 45 and 44 d, respectively; Fig. 2, C and D). Of note, five of nine mice in the combination therapy group were completely cured, and these cured mice were resistant to rechallenge with E0771 tumors (Fig. S1, C and D), suggesting induction of tumor-specific immune responses. We confirmed that cGAMP reliably activated the immune system via the STING signaling pathway, because STING-deficient ($STING^{\Delta}$) mice did not show any anti-tumor effects by the combination therapy (median survival time: 42 d for both control and combination therapy groups; Fig. 2, E and F). Because STING activation induces type I IFNs (Fuertes et al., 2013), we addressed whether type I IFNs are required for the efficacy of the combination therapy. Blockade of type I IFN signaling using an antagonistic antibody abrogated the anti-tumor effects of the combination therapy (Fig. 2, G and H; and Fig. S1 E). These findings show that intratumoral coadministration of cGAMP and anti-CD47 mAb enhances the anti-tumor effect in a STING-mediated type I IFN–dependent manner. In addition to the E0771 breast cancer cell line, the combination therapy induced tumor growth suppression and enhanced survival in mice bearing Lewis lung carcinoma (3LL) cells with high CD47 expression (median survival time: 32 d in control, 31 d in anti-CD47 mAb, 36 d in cGAMP, and not reached in combination therapy groups; Fig. 2, I and J; and Fig. S1, F and G). E0771 and 3LL cells were found to keep their CD47 expression high in vivo (Fig. S1 H).

We did not observe the therapeutic effect of anti-CD47 mAb monotherapy in E0771 and 3LL models. This is inconsistent with a previous report using MC-38 and A20 cell lines in which STING axis is required for anti-CD47–mediated anti-tumor effect (Liu et al., 2015). To explain this discrepancy, we compared the expression levels of cGAMP synthase (cGAS) and STING among three cell lines (E0771, 3LL, and MC-38). E0771 and 3LL

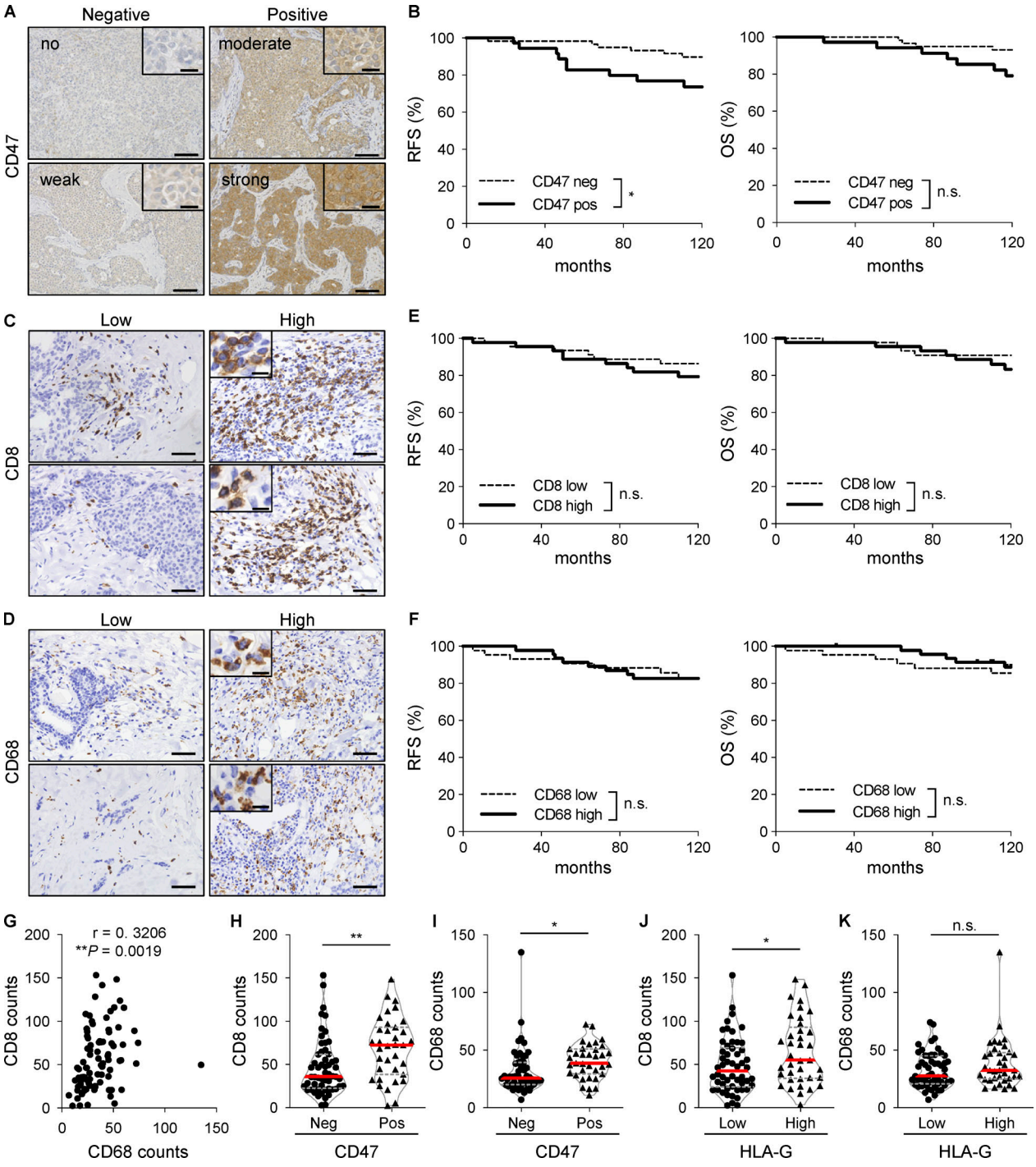

Figure 1. **CD47 is highly expressed in breast cancer specimens and significantly associated with a high infiltration of CD8⁺ and CD68⁺ cells. (A)** Representative images of human breast cancer tissues (n = 98) with no, weak, moderate, and strong expression levels of CD47. **(B)** Kaplan–Meier curves of CD47 expression in breast cancer specimens showing RFS (left panel) and OS (right panel) rates. **(C–F)** Representative images of human breast cancer tissues (n = 91) with low and high expression levels of CD8 (C) and CD68 (D). Kaplan–Meier curves of CD8 (E) and CD68 (F) expressions in breast cancer specimens showing RFS (left) and OS (right) rates. **(G)** Correlation between infiltrations of CD8⁺ and CD68⁺ cells in breast cancer specimens. **(H and I)** Associations between CD47 expression levels and CD8⁺ (H) or CD68⁺ (I) cells. **(J and K)** Associations between HLA-G expression levels and CD8⁺ (J) or CD68⁺ (K) cells. The horizontal red lines indicate medians. *, P < 0.05; **, P < 0.01; log-rank (Mantel–Cox) test (B, E, and F), Spearman rank correlation test (G), and Mann–Whitney U test (H–K). Scale bars represent 20 µm and 100 µm (A) and 10 µm and 50 µm (C and D).

Table 1. **CD47 staining patterns and clinicopathological parameters in patients with breast cancer**

Clinicopathological parameters	CD47		P value
	Negative (*n* = 62)	Positive (*n* = 36)	
Age (32–83 yr)	55 ± 11	58 ± 13	0.2448
Menopausal status			
Pre	27	11	0.2032
Post	35	25	
Nuclear grade			
1	23	12	0.7615
2	36	21	
3	3	3	
Lymphatic duct invasion			
–	48	19	**0.0115**
+	14	17	
Vascular invasion			
–	44	10	**<0.0001**
+	18	26	
Pathological T			
T1	54	27	0.0797
T2	6	9	
T3	2	0	
LN metastasis			
–	18	15	0.2221
+	43	21	
Pathological stage			
I	38	17	0.1286
II	19	18	
III	5	1	
ER			
–	10	7	0.6760
+	52	29	
PR			
–	15	11	0.4916
+	47	25	
HER2			
–	9	7	0.5246
+	53	29	
HLA-G			**0.0094**
Low	44	16	
High	18	20	
Treatment (FEC ± DOC)			
–	56	35	0.2011
+	6	1	

DOC, docetaxel; FEC, 5-fluorouracil, epirubicin, and cyclophosphamide. P < 0.05 was considered statistically significant.

had lower cGAS expression than MC-38, while STING expression was higher in E0771 and 3LL than in MC-38 (Fig. S1, I–M). Considering recent reports that cGAS in tumors triggers STING-mediated type I IFN responses (Marcus et al., 2018; Schadt et al., 2019), the efficacy of anti-CD47 mAb monotherapy would depend on the high expression of cGAS in tumors. Therefore, exogenous STING stimulation would be needed for CD47-targeting therapy in cGAS-low tumors. Collectively, these results suggest that combination treatment with cGAMP and an antagonistic anti-CD47 mAb may provide effective cancer immunotherapy in patients with various cancer types expressing high levels of CD47 regardless of cGAS expression.

To reveal the mechanism by which intratumoral STING stimulation effectively recruits $CD11b^{+}Ly6C^{+}$ monocytes/macrophages to the tumor site, we measured gene expression levels in the tumor tissue after each treatment and found that CCL2, CCL3, CCL4, CCL5, CXCL10, CXCL11, IFN-β1, and Mx1 were upregulated by cGAMP administration (Fig. S2 A). Moreover, we detected chemokine receptors CCR2, CCR5, and CXCR3 in the cGAMP-triggered tumor-migrating monocytes/macrophages (Fig. S2 B) and thus inhibited their chemokine signaling by using inhibitors for CCR2 or CCR5 and an antagonistic antibody against CXCR3. We found that none of the inhibitors blocked the migration triggered by the combination therapy (Fig. S2, C and D). Meanwhile, anti-IFN-α/β receptor 1 (anti-IFNAR1) mAb inhibited tumor-migrating monocytes/macrophages by cGAMP (Fig. 2 K). Moreover, we assessed the requirement of STING expression in monocytes/macrophages using bone marrow (BM) chimeras between WT and $STING^{\Delta}$ mice. In WT host mice, both WT and $STING^{\Delta}$-BM chimera showed increased monocytes/macrophages by cGAMP treatment; while in $STING^{\Delta}$ host mice, a similar result was found in WT, but not $STING^{\Delta}$-BM chimera (Fig. 2 L), indicating that monocytes/macrophages do not need STING expression to migrate into tumors treated with cGAMP.

Additional treatment with blockade of CD47 signaling promotes monocyte/macrophage phagocytosis of tumor cells and tumor-specific T cell priming compared with cGAMP treatment

To demonstrate how anti-CD47 mAb and cGAMP synergistically enhance the anti-tumor effect, we first addressed the impacts of these treatments on macrophages in vitro using BM-derived macrophages (BMDMs) and CFSE-labeled E0771. Anti-CD47 mAb significantly enhanced tumor phagocytosis by

Table 2. **Correlating infiltration between CD8 and CD68 in patients with breast cancer**

	CD68		P value
	Low (*n* = 44)	High (*n* = 47)	
CD8			
Low	32	14	**<0.0001**
High	12	33	

P < 0.05 was considered statistically significant.

Table 3. **Correlation between the expression of CD47 and CD8 or CD68 in patients with breast cancer**

	CD47		P value
	Negative (n = 56)	Positive (n = 35)	
CD8			
Low	35	11	**0.0039**
High	21	24	
CD68			
Low	35	9	**0.0006**
High	21	26	

P < 0.05 was considered statistically significant.

BMDM regardless of the presence of cGAMP (Fig. 3, A and B). Furthermore, enhanced phagocytosis by anti-CD47 mAb was also observed in the presence of anti-IFNAR1 mAb (Fig. 3 C) and in STING$^{\Delta}$ mouse-derived BMDM (Fig. 3 D), suggesting that anti-CD47 mAb–enhanced phagocytosis was independent of type I IFNs and STING signaling. However, cGAMP treatment up-regulated T cell priming–relating molecules such as H-2K^{b}, CD80, and CD86 in BMDM regardless of the presence of anti-CD47 mAb in a partially type I IFN–dependent manner (Fig. 3 E) and IFN-β1 induced up-regulation of these T cell priming molecules in both WT and STING$^{\Delta}$ BMDMs (Fig. S2 E). Given that tumor endothelial cells also produce IFN-β in response to cGAMP in a STING-dependent manner (Demaria et al., 2015), cGAMP-triggered type I IFN induction in nonimmune cells as well as tumor cells would be important for recruiting and activating monocytes/macrophages.

Next, we established a GFP-transduced E0771 cell line (E0771-GFP) to assess whether coadministration of anti-CD47 mAb promotes phagocytosis of tumor cells by monocytes/macrophages accumulating in tumors via intratumoral injection of cGAMP in vivo. Merged immunofluorescent images revealed that the combination therapy showed stronger yellow fluorescence than cGAMP monotherapy, indicating that GFP-expressing tumor cells were phagocytosed at higher levels by monocytes/macrophages of tumors treated with the combination therapy than those treated with cGAMP monotherapy (Fig. 3, F and G), suggesting that coadministration of anti-CD47 mAb enhances monocyte/macrophage phagocytosis of tumor cells as compared with cGAMP monotherapy in vivo. To our surprise, anti-CD47 mAb monotherapy only slightly enhanced tumor phagocytosis by F4/80^{+} tumor-associated macrophages. This may be one reason why anti-CD47 monotherapy did not show any anti-tumor effects in our experimental setting. Furthermore, we found that cGAMP monotherapy and the combination therapy up-regulated H-2K^{b} and CD80 in CD11b^{+}Ly6C^{+} monocytes/macrophages as well as in the in vitro experiments that excluded CD86 (Fig. 3 H). In addition, we addressed whether these phagocytosis-enhanced monocytes/macrophages efficiently activated tumor-specific T cells ex vivo. To evaluate tumor-derived antigen-specific T cell responses, we established an OVA-encoding gene-transduced E0771 cell line (E0771-OVA; Fig. S2 F). Monocytes/macrophages were sorted from tumor tissues of E0771-OVA–bearing mice receiving each therapy (Fig. 3 I) and cocultured with OT-I–derived CD8^{+} T cells (OT-I cells), and then IFN-γ–producing cell numbers were assessed by ELISpot assay. We found that monocytes/macrophages from combination-treated mice induced more IFN-γ–producing OT-I cells compared with those from cGAMP-treated mice (Fig. 3 J). In contrast, there were no responses in cocultured OT-I cells with monocytes/macrophages from control or anti-CD47 mAb-treated mice, supporting the results shown in Fig. 3 G. Taken together, these results suggest that cGAMP-derived tumor-infiltrating monocytes/macrophages enhance phagocytosis of tumor cells and the activation of tumor-reactive T cells by coadministration of anti-CD47 mAb.

Combination treatment with cGAMP and anti-CD47 mAb increases the number of activated T cells and induces systemic anti-tumor immunity

Because cured mice rejected the rechallenge with cognate tumor cells as mentioned above (Fig. S1 D), we addressed the contribution of T cells to the efficacy of the combination therapy. We found that CD4 depletion delayed tumor growth and prolonged survival (Fig. S3, A–C), consistent with a previous report (Sánchez-Paulete et al., 2018). However, more completely cured mice were observed in the combination group than in the control group. Meanwhile, depleting CD8^{+} T cells totally abolished the anti-tumor effects of the combination therapy (median survival time: 48.5 d in control, 57 d in combination + isotype control Ab, and 44.5 d in combination + anti-CD8 mAb groups; Figs. 4 A and S3 D). These data indicate that the combination therapy effectively activated tumor-specific CD8^{+} T cell responses. Treatment with cGAMP and anti-CD47 mAb had an additional effect on increasing the percentage of CD4^{+} T cells and led to a synergistic increase in CD8^{+} T cells among TILs (Fig. 4 B). We therefore addressed the responsible chemokine signaling for T cell migration into tumors treated with the combination therapy. Because the migrating T cells expressed CCR2, CCR5, and CXCR3 (Fig. 4 C), we blocked their chemokine signaling by using inhibitors for CCR2 or CCR5 and an antagonistic antibody for CXCR3. The combination therapy–triggered migration of both T cell subsets was significantly suppressed by CCR5, but not CCR2, inhibitor (Fig. 4 D). There was a biological trend of an effect similar to our previously observed inhibition by anti-CXCR3 mAb (Harabuchi et al., 2020; Fig. 4 E). We then analyzed tumor-draining LNs (TDLNs) and found that the combination therapy efficiently activated both CD4^{+} and CD8^{+} T cells in addition to increasing the number of T cells in TDLNs (Fig. S3 E). In addition, although there was no difference in total T cell number among the groups in contralateral LNs (CLNs; Fig. S3 F), the combination therapy had an additional effect on increasing the number of CD8^{+}CD69^{+} T cells, while cGAMP monotherapy, but not anti-CD47 mAb monotherapy, up-regulated the expression of CD69 in CD4^{+} T cells. Furthermore, to evaluate tumor antigen-specific T cell responses, we i.v. transferred CFSE-labeled CD45.1^{+}OT-I cells into E0771-OVA–bearing mice, which simultaneously received each treatment, and collected TDLNs, CLNs, and spleen to analyze the OT-I cell responses (Fig. S3 G).

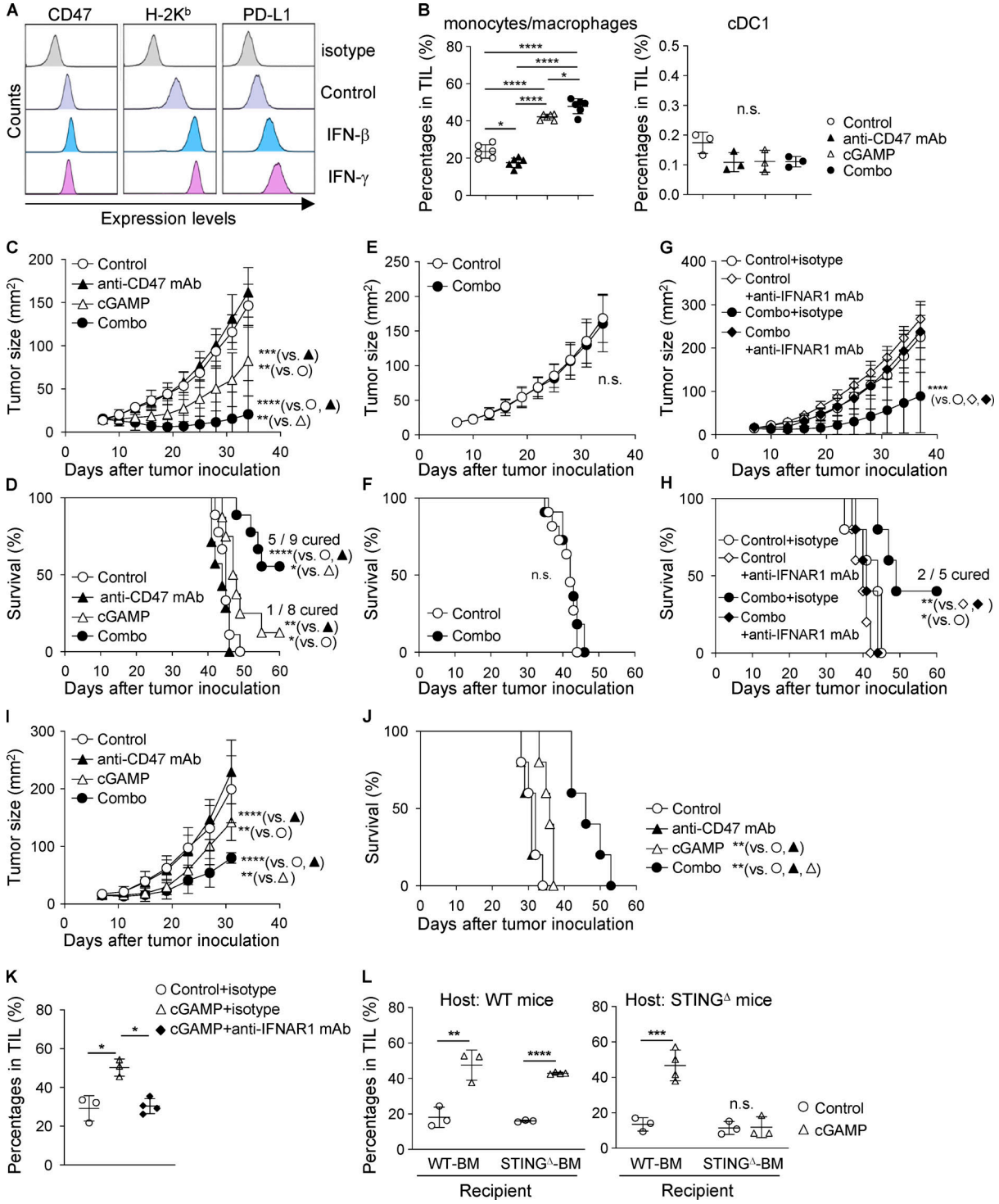

Figure 2. **Intratumoral coinjection of cGAMP and anti-CD47 mAb efficiently suppresses tumor growth and prolongs survival in a STING- and type I IFN–dependent manner. (A)** Expression levels of CD47, H-2K^b, and PD-L1 in E0771 cells treated with rIFN-β and rIFN-γ for 48 h in vitro. Data are representative of three independent experiments. **(B)** Percentage of CD11b$^+$Ly6C$^+$ monocytes/macrophages (left) and cDC1 (right) in TILs at 24 h after intratumoral treatment with anti-CD47 mAb and/or cGAMP (n = 3; data are representative of two independent experiments). **(C–F)** E0771-bearing WT mice (C and D) or STING$^{\Delta}$ mice (E and F) were treated with intratumoral injection of anti-CD47 mAb and/or cGAMP on day 7 after tumor inoculation and monitored for tumor size (C and E) and survival rates (D and F; n = 7–9 mice/group for C and D; n = 11–12 mice/group for E and F). Data represent two independent experiments. **(G and H)** E0771-bearing WT mice received intratumoral injection of anti-CD47 mAb and cGAMP on day 7 after tumor inoculation. They were also treated with i.p. injections of anti-IFNAR1 mAb or its isotype control on days 7 and 14 and monitored for tumor size (G) and survival rates (H; n = 5 mice/group). Data are representative of two independent experiments. **(I and J)** Tumor size (I) and survival rates (J) of 3LL-bearing WT mice receiving the same treatment as described above (n = 5 mice/group). Data are representative of two independent experiments. **(K and L)** Percentage of CD11b$^+$Ly6C$^+$ monocytes/macrophages in TILs at 24 h after intratumoral treatment with control or cGAMP (n = 3–4; data are representative of two independent experiments). Mice were simultaneously

treated with i.p. injection of anti-IFNAR1 mAb or its isotype control (K). BM chimeras were generated by i.v. injecting BM of WT or STING$^{\Delta}$ mice into γ-irradiated WT (left panel) and STING$^{\Delta}$ (right panel) mice (L). Data are shown as mean ± SD. *, P < 0.05; **, P < 0.01; ***, P < 0.001; ****, P < 0.0001; two-way (B, C, G, and I) and one-way (K) ANOVA with interaction followed by Tukey's multiple comparison test, unpaired *t* test (E and L), and log-rank (Mantel–Cox) test (D, F, H, and J).

Although cGAMP treatment significantly enhanced OT-I cell proliferation even in E0771 parent–bearing mice compared with control and anti-CD47 mAb monotherapy treatments, the combination therapy significantly promoted OT-I cell proliferation in all tissues of E0771-OVA–bearing mice compared with the other treatments (Fig. 4 F). The enhanced OT-I cell proliferation by the combination therapy was specific for the tumor antigen, because this was not observed in E0771-parent–bearing mice. Moreover, OT-I cells highly produced IFN-γ in TDLNs of mice receiving the combination therapy compared with other treatments (Fig. 4 G).

Because our findings suggested that the combination of anti-CD47 mAb and cGAMP therapy could efficiently enhance systemic anti-tumor immunity, we assessed this possibility by using a two-tumor mouse model in which mice were inoculated with E0771 cells into both left and right mammary fat pads and only the left-sided tumor received cGAMP with or without anti-CD47 mAb treatment, as shown in Fig. 5 A. We did not evaluate anti-CD47 mAb monotherapy in this two-tumor model, because it did not show an anti-tumor effect, even in the single-tumor model. Predictably, the combination therapy significantly inhibited tumor growth compared with control treatment in both treated (left) and untreated (right) tumors; however, cGAMP monotherapy did not show any anti-tumor effect, even in the treated (left) tumor (Fig. 5 B; and Fig. S4, A and B). Furthermore, the combination therapy prolonged survival compared with control and cGAMP treatments, and two of eight mice in the combination group completely rejected both treated and untreated tumors (Fig. 5 C). In this two-tumor model, although there were no differences in cDC1 percentages among tumor tissues, CD11b^{+}Ly6C^{+} monocytes/macrophages were highly recruited to only the treated tumors with both cGAMP monotherapy and the combination therapy (Fig. 5 D), in which the expression levels of chemokines and IFN-β1 were obviously upregulated, while they were not in the untreated tumors (Fig. S4 C). Given these findings, we hypothesized that the difference in efficacy between cGAMP monotherapy and the combination therapy would be caused by the activation status of T cells in TDLNs. We observed significantly increased numbers of CD8^{+}CD69^{+}, but not CD4^{+}CD69^{+}, T cells in treated (left) TDLNs with the combination therapy compared with those with cGAMP monotherapy, although there was no difference in T cell numbers in treated (left) TDLNs between the two groups (Fig. S4, D and E). Moreover, in untreated (right) TDLNs, the combination therapy increased numbers of not only CD69-positive T cells but also total T cells (Fig. S4, F and G) compared with cGAMP monotherapy. To gain a better understanding of T cell function in TDLNs, TDLN cells were cocultured with E0771 tumors, and IFN-γ production was evaluated. B16F10 cells were used as an irrelevant stimulus. In treated (left) TDLNs, although IFN-γ was produced in response to E0771 cells in both groups treated with cGAMP monotherapy and the combination therapy, the combination therapy induced higher IFN-γ production than cGAMP monotherapy (Fig. S4 H). By contrast, in untreated (right) TDLNs, E0771-specific IFN-γ production was observed in the group treated with the combination therapy, but not in the group treated with cGAMP monotherapy (Fig. S4 I). In addition, we observed that OT-I cell responses were enhanced in both treated and untreated TDLNs in the combination, but not cGAMP, group (Fig. 5, E and F). Taken together, these findings suggest that combination therapy using cGAMP and anti-CD47 mAb enhanced both local and systemic tumor-specific anti-tumor immune responses.

Low expression level of cGAS is associated with poor prognosis in patients with high infiltration of CD8^{+} cells

Since cGAS contributes to inflammation of the tumor microenvironment via activating STING signaling autonomously, which is required for the efficacy of CD47-targeting therapy (Schadt et al., 2019), we evaluated the expression of cGAS and STING in 89 breast cancer specimens by IHC. The results of the initial evaluation showed that 4, 16, 23, and 46 patients were classified as having no, weak, moderate, and strong staining for cGAS, respectively, and 34, 20, 17, and 18 for STING, respectively (Fig. 6, A and B). Furthermore, the patients were grouped into negative (no and weak staining) and positive (moderate and strong staining) expression specimens (20 and 69 patients for cGAS, respectively, and 54 and 35 for STING, respectively). There were no significant differences in OS between the expression levels of cGAS or STING (Fig. 6, C and D). We also found that cGAS^{neg}CD8^{high} patients showed significantly poor OS compared with other patients (Fig. 6 E). We did not observe any significant differences with the combination of cGAS and CD68 (Fig. 6 F).

Discussion

The results presented here demonstrate the efficacy of a novel anti-tumor immunotherapy using cGAMP and anti-CD47 mAb for the treatment of tumors with high expression of CD47. Current studies show that STING agonists induce anti-tumor immune responses (Fuertes et al., 2013; Gajewski et al., 2013; Ishikawa et al., 2009), and we also demonstrated that intratumoral injection of the STING ligand cGAMP resulted in monocyte/macrophage accumulation in the tumor microenvironment, which contributes to anti-tumor activities (Ohkuri et al., 2017). However, myeloid cells are generally known to infiltrate intensively in the tumor microenvironment and play a role in promoting tumor growth and suppressing anti-tumor immunity. SIRPα is an inhibitory receptor expressed on myeloid cells, including monocytes/macrophages, and CD47 is its receptor, which is overexpressed in various cancer types (Willingham et al., 2012). Based on our IHC analysis showing that CD47 was highly expressed in 36.7% of breast cancer

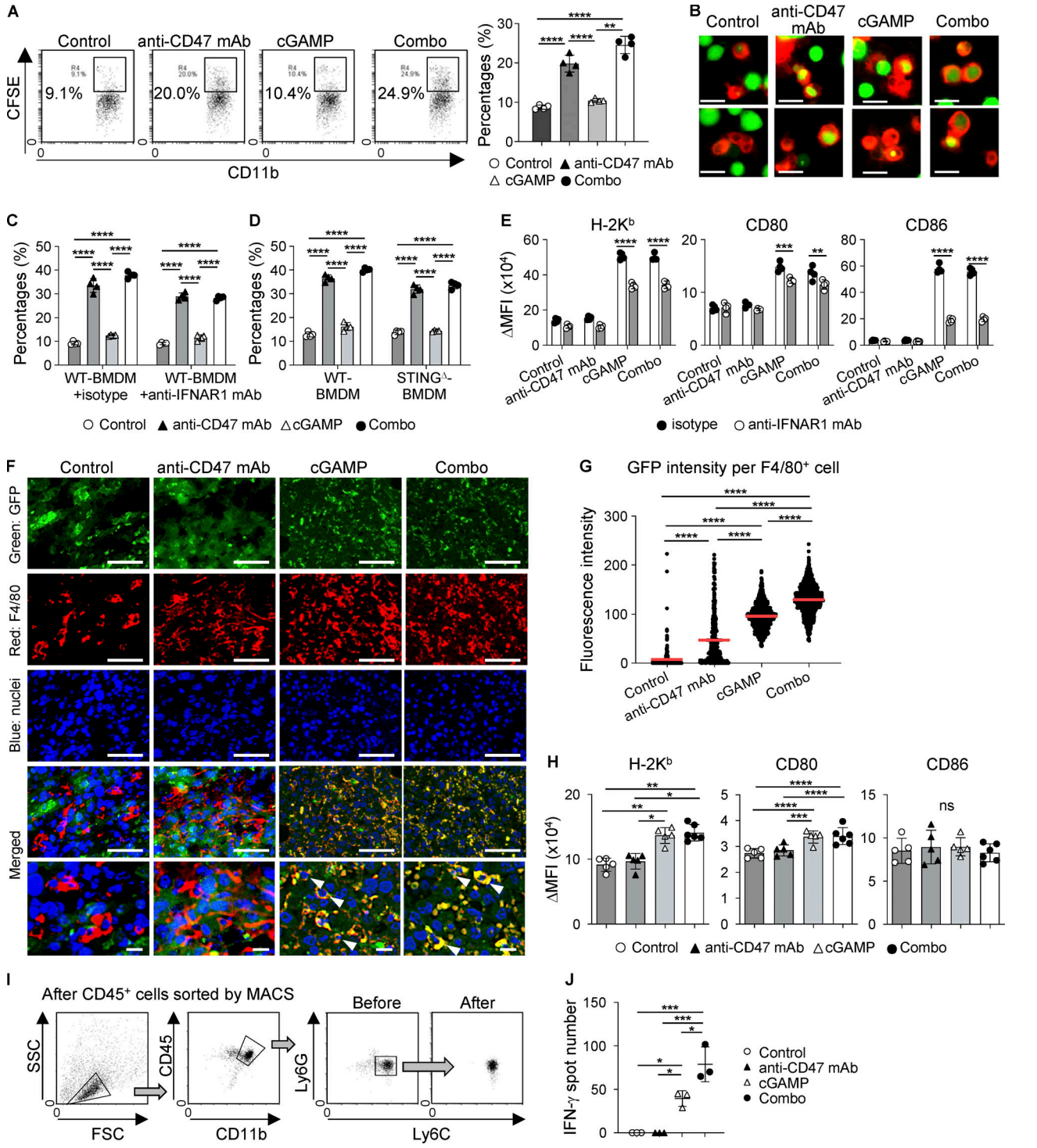

Figure 3. **Enhanced phagocytosis of tumor cells and tumor-specific CD8⁺ T cell priming in the tumor microenvironment following combined cGAMP treatment with CD47 blockade. (A–D)** BMDMs of WT (A, C, and D), C57BL/6-tdTomato (B), and STING$^{\Delta}$ (D) mice were cocultured with CFSE-labeled E0771 cells in the presence of anti-CD47 mAb and/or cGAMP for 4 h (n = 4; data are representative of two independent experiments). Phagocytosis was assessed using a flow cytometer (A, C, and D) and microscope (B). Isotype control or anti-IFNAR1 mAbs were added (C). **(E)** Expression levels of H-2K^{b}, CD80, and CD86 in WT-BMDM after 24-h culture with E0771 cells in the presence of anti-CD47 mAb and/or cGAMP with isotype control or anti-IFNAR1 mAb (n = 4; data are representative of two independent experiments). **(F–H)** E0771-GFP-bearing WT mice were intratumorally treated with intratumoral injection of anti-CD47 mAb and/or cGAMP. After 24 h, each tumor tissue was collected. Immunofluorescence staining for tumor cells (GFP, green) and monocytes/macrophages (F4/80, red) was performed, and nuclei were stained with DAPI (blue). Merged images show monocyte/macrophage phagocytosis of tumor cells. Bottom images are high-power fields, and arrowheads indicate GFP and F4/80 double-positive cells (F). Monocyte/macrophage phagocytosis of tumors was quantified by calculating GFP fluorescence intensity per RFP⁺ cell using Hybrid Cell Count BZ-H3C software. The horizontal red lines indicate means (G; n = 3; data are representative of two independent experiments). After single-cell preparations from the collected tumor tissues by enzymatic treatment, the expression levels

of H-2K^b, CD80, and CD86 on the cell surfaces of monocytes/macrophages were evaluated using a flow cytometer (H; *n* = 5 mice from two independent experiments). **(I and J)** E0771-OVA–bearing mice were intratumorally treated with anti-CD47 mAb and/or cGAMP. After 24 h, CD11b$^+$Ly6C$^+$ monocytes/macrophages were sorted from single-cell suspensions prepared from each tumor tissue using a cell sorter following isolation of CD45$^+$ cells by a MACS magnetic system. The sorting strategy and purity are shown I. The sorted monocytes/macrophages were cocultured with OT-I cells for 24 h. IFN-γ–producing T cell numbers were evaluated by ELISpot assays (J; data are representative of two independent experiments). Change in mean fluorescence intensity (ΔMFI) against isotype control was calculated (target MFI minus control; E and H). Data are shown as mean ± SE (A, C, D, E, and J) or SD (H). *, P < 0.05; **, P < 0.01; ***, P < 0.001; ****, P < 0.0001; two-way (A, C, D, E, H, and J) and one-way (G) ANOVA followed by Tukey's multiple comparisons test. Scale bars represent 20 µm (B) and 50 µm and 10 µm (F).

specimens and that CD47 overexpression seemed to be associated with poor prognosis, we hypothesized that the CD47 molecule contributes to the suppression of anti-tumor immune responses in the breast tumor microenvironment. We therefore tested whether additional treatment by CD47-SIRPα blockade could enhance the anti-tumor effects of STING agonist treatment using a mouse breast cancer model. We confirmed that blockade of CD47-SIRPα signaling in the tumor microenvironment promoted anti-tumor responses of cGAMP by enhancing the phagocytosis of tumor cells and the activation of tumor-reactive T cells.

Recently, Alspach et al. proposed an important role for both CD4$^+$ and CD8$^+$ T cells in anti-tumor immune responses, even in the absence of MHC class II molecules on tumor cells. In addition, they claim that activation of CD4$^+$ T cells must also occur in the tumor microenvironment not only for priming of CD8$^+$ T cells but also for collaboration with CD8$^+$ T cells to maintain an effective anti-tumor immune response (Alspach et al., 2019). Our data suggest that tumor-infiltrating monocytes/macrophages induced by cGAMP and anti-CD47 mAb combination treatment show increased phagocytosis and activation of both CD4$^+$ and CD8$^+$ T cells. Although CD4 depletion improved the efficacy of the combination therapy, this is most likely attributable to the depletion of regulatory T cells (Sánchez-Paulete et al., 2018; Yu et al., 2005). Therefore, it would be important to develop a specifically regulatory T cell–targeting drug.

We previously reported that high expression of HLA-G, which is a nonclassical MHC class I molecule with immune suppressive activity, is correlated with a poor prognosis of breast cancer patients (Ishibashi et al., 2016). In this study, we showed that CD47 may serve as a poor prognosis marker in breast cancer patients as well, and its expression is associated with HLA-G. In addition, we found that CD8$^+$ cell infiltration was positively associated with expressions of CD47 and HLA-G. This may indicate that CD8$^+$ T cells help tumors escape the immune system by providing acquired immune resistance via producing TNF-α and IFN-γ, which are known to up-regulate CD47 (Betancur et al., 2017) and HLA-G (Ishibashi et al., 2016) in tumor cells, respectively. The acquired immune resistance may be implicated in poor prognosis of the patients who showed high infiltration of CD8$^+$ cells in a cGAS-low tumor, which would be low immunogenic.

Although it has been reported that CD47 expression is not associated with OS in ER$^+$ breast cancer (Cook and Soto-Pantoja, 2017), our findings are consistent with previous reports that CD47 expression is correlated with poor-prognosis molecular subtypes, such as basal and Her2/Neu-positive tumors (Zhao et al., 2011), and decreased OS in patients with breast cancer (Baccelli et al., 2014; Zhang et al., 2015). Moreover, higher levels of CD47 mRNA expression are associated with a decreased probability of progression-free survival and OS in other solid tumor types, including ovarian cancer, gliomas, and glioblastomas, as well as in hematologic tumors (Chao et al., 2010; Majeti et al., 2009; Willingham et al., 2012). These findings suggest that CD47 is a favorable target for anti-tumor immunotherapy in various cancer types. Indeed, many clinical and preclinical studies of CD47-SIRPα blockade in both solid and hematologic cancers are currently underway (Russ et al., 2018; Sikic et al., 2019).

While CD47 ligation induces cell death, CD47 blocking agents have been also proposed to enhance phagocytosis and T cell priming, and there are several reports of the improved anti-tumor efficacy of CD47 blockade when combined with anti-CD20 mAb, CD40 agonist, anti-PD-L1 mAb, or sorafenib (Chao et al., 2010; de Silva et al., 2020; Lo et al., 2015; Pan et al., 2019). Based on those results, multiple clinical studies are conducted to assess the safety and efficacy of the combination of CD47-SIRPα inhibitors with other anticancer drugs, such as molecular targeted drugs and chemotherapy. More recently, it has been shown that gut microbiota in tumor sites facilitates the anti-tumor efficacy of anti-CD47 treatment through STING signaling (Shi et al., 2020), which is consistent with previous studies demonstrating that STING signaling is required for inducing the anti-tumor response of CD47 blockade (Liu et al., 2015; Xu et al., 2017). We also showed that the therapeutic efficacy of anti-CD47 mAb would rely on cGAS expression in tumors, and this may be the reason for the requirement of exogenous STING stimulation in cGAS-low tumors, such as E0771 and 3LL. Meanwhile, inconsistent with our results, anti-CD47 mAb monotherapy has been shown to delay tumor growth even in E0771-bearing mice (Shuptrine et al., 2017). We attribute this discrepancy to differences in dose and/or frequency of anti-CD47 mAb, because they i.p. administered the antibody (Vx1000R) with 133 µg three times a week, while we intratumorally injected anti-CD47 mAb (MIAP301) with 5 µg just once. In addition, cGAS-low tumor cells establish low-immunogenic tumors where tumor-associated macrophages are predominantly polarized into M2 macrophages. Considering that anti-CD47 mAb-induced phagocytosis by M2 macrophages is less prominent than that by M1 macrophages (Zhang et al., 2016), anti-CD47 mAb would not effectively promote tumor phagocytosis by macrophages in an especially low-immunogenic tumor microenvironment, as seen in our in vivo phagocytosis analysis. In contrast, anti-CD47 mAb enhanced tumor phagocytosis by GAMP-triggered freshly migrating monocytes/macrophages in the tumor. Therefore, for anti-CD47 mAb therapy to be effective, the existence of

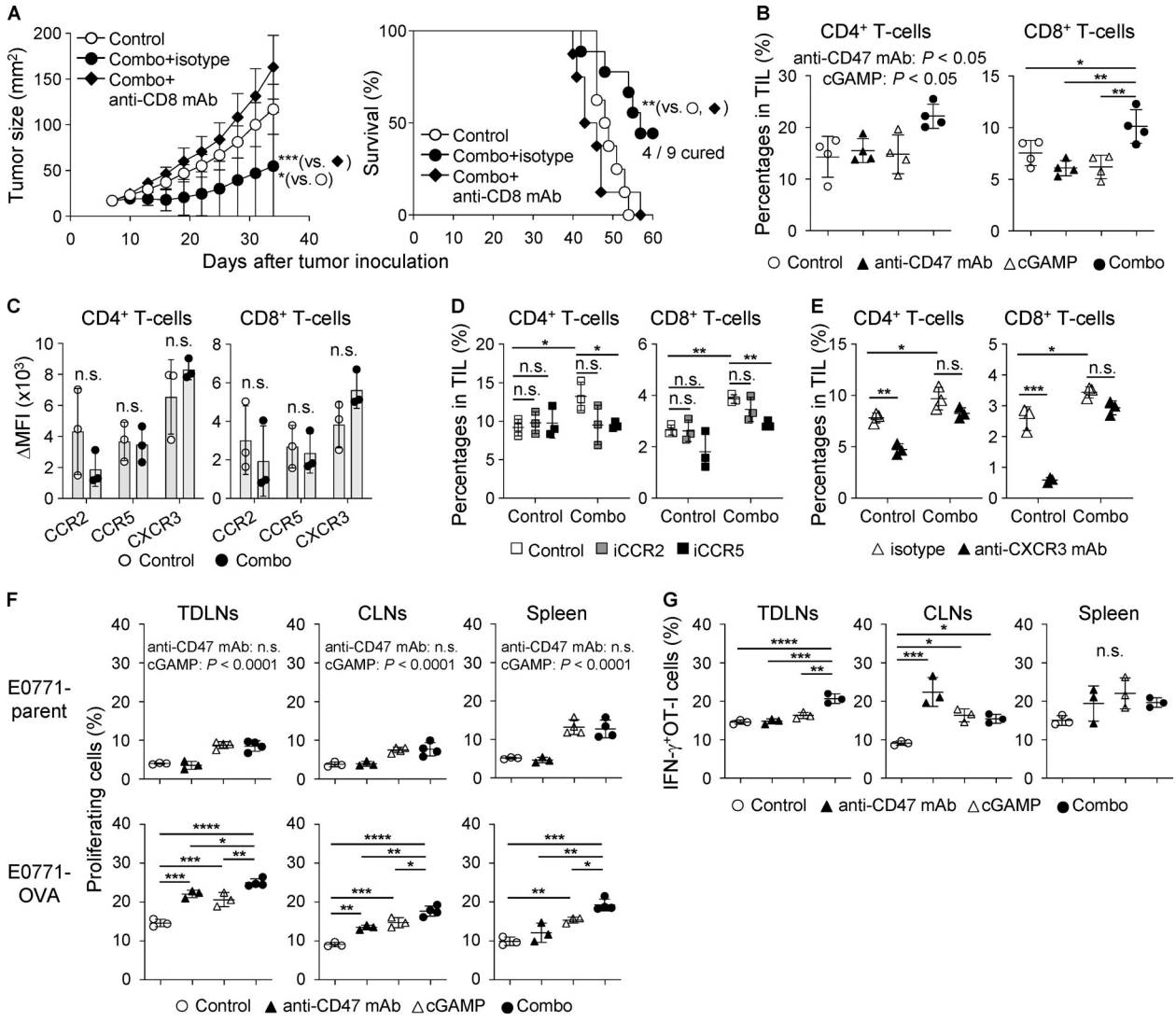

Figure 4. **Enhanced CD8⁺ T cell responses in mice treated with combination therapy. (A)** E0771-bearing WT mice were treated with intratumoral injection of anti-CD47 mAb and/or cGAMP on day 7 after tumor inoculation. Isotype control or anti-CD8 mAb was injected i.p. into mice on days 6, 13, and 20. Tumor size (left) and survival rates (right) are shown (n = 8–9 mice/group). Data represent two independent experiments. **(B–E)** After 48 h of intratumoral treatment, each tumor tissue was collected for T cell analysis (n = 3–4; data are representative of two independent experiments). Percentage of CD4⁺ and CD8⁺ T cells (B) and their expression levels of chemokine receptors (C) were evaluated using a flow cytometer. ΔMFI against isotype control was calculated (target MFI minus control). Inhibitors for CCR2 and CCR5 (iCCR2 and iCCR5, respectively) and their vehicle control were i.p. injected into mice followed by intratumoral treatments (D). Blocking antibody for CXCR3 (anti-CXCR3 mAb) was i.p. administered to mice 2 h before intratumoral treatment. Isotype antibody was used as a control (E). **(F and G)** E0771-parent– or E0771-OVA–bearing WT mice were treated with intratumoral injections of anti-CD47 mAb and/or cGAMP on day 7 after tumor inoculation, following the transfer of CD45.1⁺OT-I cells. 4 d later, TDLNs, CLNs, and spleen were collected. Proliferation (F) and IFN-γ production (G) of the transferred OT-I cells were assessed (n = 3–4; data are representative of two independent experiments). Data are shown as mean ± SD. *, P < 0.05; **, P < 0.01; ***, P < 0.001; ****, P < 0.0001; two-way (A, left; B, E, F, and G) and one-way (D) ANOVA with interaction followed by Tukey's multiple comparison test, unpaired t test (C), and log-rank (Mantel–Cox) test (A, right).

monocytes/macrophages with phagocytic activity in the tumor microenvironment is important. These findings suggest that intratumoral cGAMP treatment would help to overcome hurdles in anti-CD47 mAb monotherapy by inducing inflammatory cytokines and recruiting M1-like monocytes/macrophages to the tumor site (Ohkuri et al., 2017) and that the combination therapy of cGAMP and anti-CD47 mAb could show a synergistically anti-tumor effect.

Contrary to previous reports showing that monocytes/macrophages migrate into inflammatory sites via CCL2/CCR2 signaling (Bakst et al., 2017; Wu et al., 2018), we could not suppress their migration into the treated tumor tissues with the combination therapy using a CCR2 inhibitor. Instead, we demonstrated, using anti-IFNAR1 mAb and BM-chimeric mice, that their tumor migration depended on type I IFNs, which would be induced in nonimmune cells in the tumor site. These findings indicate that an important role of intratumoral cGAMP treatment would be to induce robust type I IFNs in the tumor microenvironment, thereby recruiting M1-like monocytes/macrophages there.

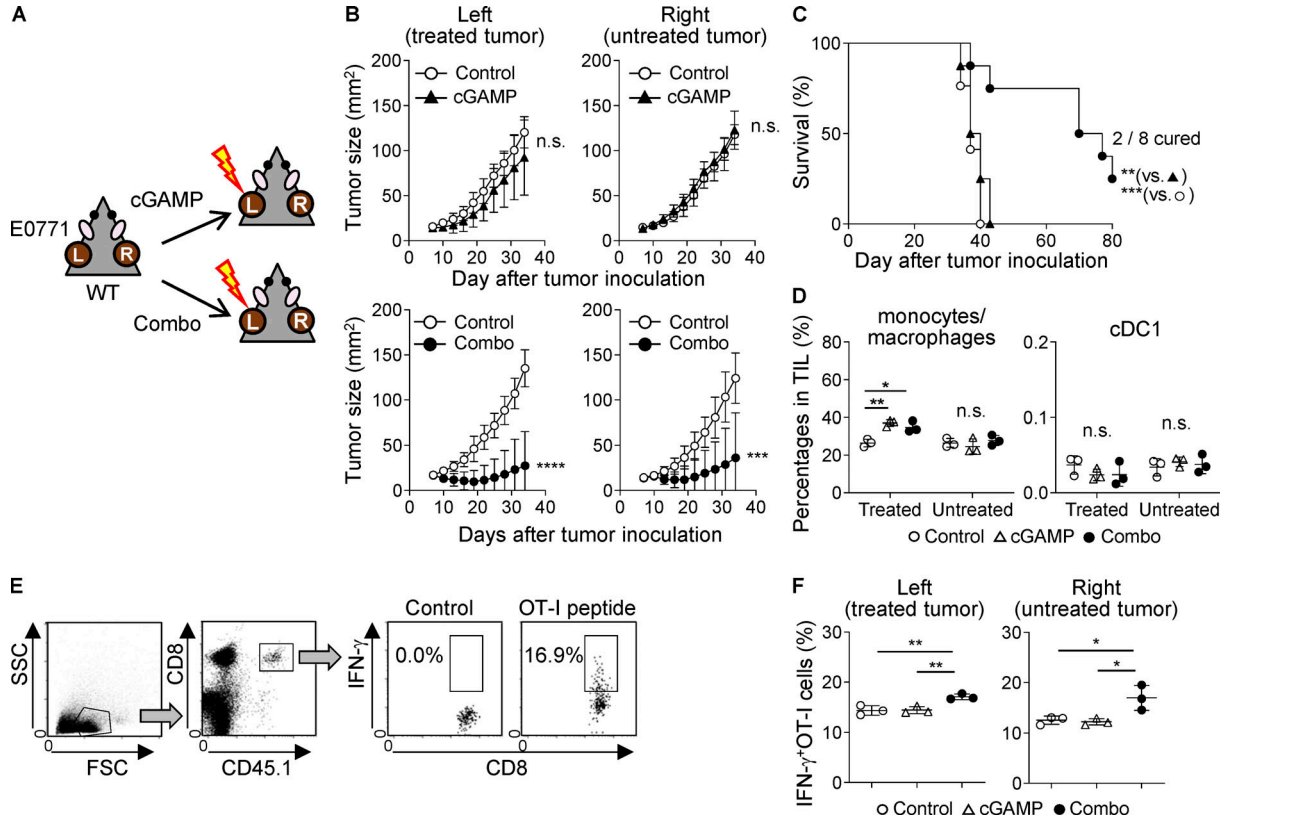

Figure 5. **Combination therapy with cGAMP and anti-CD47 mAb systemically activates anti-tumor immunity. (A)** Schema of the two-tumor mouse model. L, treated tumor; R, untreated tumor. **(B and C)** Tumor size (B) and survival (C) of E0771 two-tumor–bearing mice treated with cGAMP monotherapy (upper panels) or the combination therapy (lower panels) compared with control treatment (n = 8–9; data represent two independent experiments). The treatment schedule was the same as described in Fig. 2. **(D)** Percentage of infiltrating monocytes/macrophages (left) and cDC1 (right) in the treated and untreated tumor tissues at 24 h after treatment with cGAMP or the combination (n = 3; data are representative of two independent experiments). **(E and F)** E0771-OVA–bearing WT mice were treated with intratumoral injection of cGAMP or the combination in their left flanks on day 7 after tumor inoculation, following the transfer of CD45.1⁺OT-I cells. 4 d later, TDLNs were collected, and the transferred OT-I-cell responses were assessed using a flow cytometer. The gating strategy for CD45.1⁺OT-I cells (E) and the percentage of IFN-γ–producing OT-I cells in response to the OT-I peptide (SIINFEKL; F) are shown (n = 3; data are representative of two independent experiments). Data are shown as mean ± SD. *, P < 0.05; **, P < 0.01; ***, P < 0.001; ****, P < 0.0001; unpaired t test (B), log-rank (Mantel–Cox) test (C), and one-way ANOVA with Tukey's multiple comparison test (D and F).

Because CD47 is also expressed in normal cells in addition to tumor cells to mediate the "don't eat me" signal to phagocytic cells, there is a potential risk of undesirable side effects such as hemophagocytic syndrome and anemia when CD47-SIRPα signaling is systemically blocked. A phase 1 trial of anti-CD47 mAb showed that the most common adverse event was expected on-target anemia (Sikic et al., 2019). In this regard, local administration of anti-CD47 mAb might be more appropriate than systemic administration, even though anemia caused by systemic treatment with anti-CD47 mAb was mild and transient.

Recent studies have shown the efficacy of intratumoral administration of STING agonists in mouse tumor models, and several mechanisms by which STING agonists promote anti-tumor responses have been proposed, such as induction of type I IFNs that activate dendritic cells to facilitate T cell priming and infiltration of activated natural killer and T cells into tumors. In the present study, the intratumoral coinjection of cGAMP and anti-CD47 mAb showed anti-tumor effect for the untreated tumor in the two-tumor model and enhanced the OT-I cell responses systemically, suggesting induction of effective anti-tumor immunity. Interestingly, STING-targeting therapy enhanced OT-I cell proliferation independently of the tumor antigen. This could be caused by homeostatic cytokines IL-12 or IL-15 (Kieper et al., 2001; Zhang et al., 1998), which are produced from myeloid cells by exposure to type I IFNs (Gautier et al., 2005; Nguyen et al., 2002). Inducing these cytokines would be one of the benefits of STING-targeting therapy, although further studies are needed. cDC1 would also contribute to the anti-tumor effect of the combination therapy, because STING-dependent type I IFN production activates cDC1 to cross-present tumor antigens to CD8⁺ T cells (Diamond et al., 2011; Fuertes et al., 2011). Moreover, as reviewed by Grabowska et al. (2018), CD11b⁺Ly6C⁺ monocytes/macrophages might enhance anti-tumor immune responses in cooperation with cDC1. Hence, in addition to STING agonist monotherapy, combination therapies with other treatments that activate T cells and/or DCs (e.g., tumor vaccines, radiotherapy, and immune checkpoint inhibitors) enhance anti-tumor immunity more effectively (Baird et al., 2016; Corrales et al., 2015; Demaria et al., 2015; Foote et al., 2017; Sallets et al., 2018). Based on our previous findings that intratumoral injection

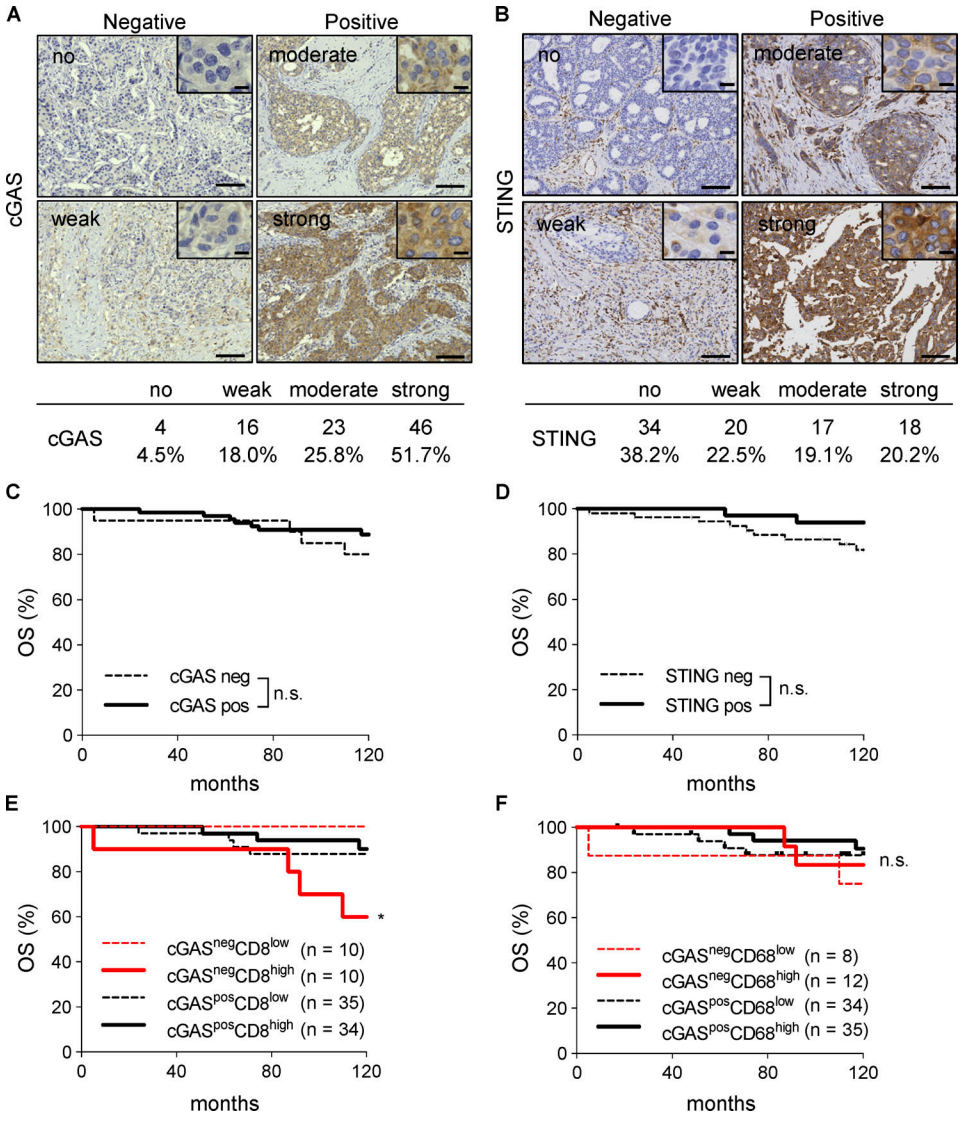

Figure 6. **Low expression level of cGAS is associated with poor prognosis in patients with high infiltration of CD8⁺ cells. (A and B)** Representative images of human breast cancer specimens (n = 89) with no, weak, moderate, or strong expression levels of cGAS (A) and STING (B). The numbers and percentages of each expression level are shown under the images. **(C and D)** Kaplan–Meier curves of cGAS (C) and STING (D) expression in breast cancer specimens showing OS rates. **(E and F)** Kaplan–Meier curves of combined cGAS and CD8 (E) or cGAS and CD68 (F) expression in breast cancer specimens showing OS rates. *, P < 0.05; log-rank (Mantel–Cox) test. Scale bars, 10 µm and 100 µm.

of cGAMP induces the transient accumulation of monocytes/macrophages in the tumor microenvironment (Ohkuri et al., 2017), we demonstrated in this study that intratumoral coadministration of a STING ligand and anti-CD47 mAb effectively activated anti-tumor immune responses. Therefore, when combined with STING agonists, other monocyte/macrophage-modulating drugs might show more potent anti-tumor activity, as observed with anti-CD47 mAb.

In summary, the combination treatment of cGAMP and an antagonistic anti-CD47 mAb induces effective anti-tumor immune responses against tumors with CD47 overexpression through activation of monocyte/macrophage phagocytosis and tumor-specific T cells. This combination therapy also leads to memory and systemic anti-tumor immune responses, suggesting an effective therapeutic strategy.

Materials and methods

Clinical samples

Tumor tissue samples were obtained from patients with breast cancer by surgical resection at Asahikawa Medical University Hospital. This study was approved by the Research Ethics Committee of Asahikawa Medical University (approval no. 19214) and was performed in accordance with the Declaration of Helsinki. Written informed consent was obtained from all patients who provided tissue samples.

IHC

IHC analysis of breast cancer specimens and mouse tumor and normal tissues was performed using the EnVision HRP System (K5361; Dako). Formalin-fixed sections were obtained from breast cancer patients. Samples were boiled in EDTA buffer

(pH 9.0) for antigen retrieval, and endogenous peroxidase activity was inhibited according to the manufacturer's instructions. Sections were then incubated with mouse anti-human CD47 (n = 98; clone BRIC126; Bio-Rad), anti-human CD8 (clone C8/144B, 1:100; Dako), anti-human CD68 (clone PG-M1, 1:150; Abcam), anti-human cGAS (clone D-9, 1:600; Santa Cruz Biotechnology), anti-human STING (clone D2P2F, 1:400; Cell Signaling Technology), or anti-mouse CD47 (clone MIAP301, 1:50; Bio X Cell) mAbs at a dilution of 1:50 overnight at 4°C, followed by incubation with an HRP-conjugated secondary antibody and substrate. In some experiments described below, mouse tumor tissues were collected after 24-h intratumoral treatment and fixed with 4% paraformaldehyde, and 2-µm-thick sections were taken from formalin-fixed paraffin-embedded tissue blocks. Sections were immunostained with rat anti-GFP polyclonal antibody (1:1,000; MBL) and rat anti-mouse F4/80 mAb (1:20; clone C1:A3-1; Cedarlane Laboratories) and visualized using Histofine Simple Stain MAX PO (Nichirei Biosciences) and the Vectastain ABC Elite kit (Vector Laboratories), respectively. The nucleus was stained with DAPI (Sigma). Images were acquired using a BZ-X700 microscope (Keyence), and monocyte/macrophage phagocytosis of tumors was quantified by calculating GFP fluorescence intensity per F4/80$^+$ cell using Hybrid Cell Count BZ-H3C software (Keyence). Each tissue section of breast cancer was examined in a blinded manner by three pathologists independently and classified into four grades based on the intensity of expression for CD47, cGAS, and STING (no, weak, moderate, and strong), followed by two clusters (negative, no and weak staining; and positive, moderate and strong staining). For CD8$^+$ and CD68$^+$ cells, patients were classified into two groups (low and high) according to counts of each positive cell (lower and higher than the average of all specimens analyzed).

Cell lines and mice

The E0771 mouse breast cancer and the mouse 3LL cell lines were purchased from CH3 BioSystems and JCRB Cell Bank, respectively. The MC-38 mouse colon adenocarcinoma cell line was purchased from Kerafast. The cells were cultured in RPMI 1640 medium (Nacalai Tesque) supplemented with 10% fetal bovine serum (Biowest), penicillin (100 U/ml; Meiji Seika Pharma), and streptomycin (100 µg/ml; Meiji Seika Pharma). To establish GFP- and OVA-expressing E0771 cell lines (E0771-GFP and E0771-OVA, respectively), E0771 cells were transfected with pcDNA3-EGFP or pcDNA3-OVA plasmids (Addgene) and Lipofectamine LTX Reagent with Plus Reagent (Thermo Fisher Scientific) and selected with G418 (Wako) for the expression of each transgene. C57BL/6J WT, B6.129(Cg)-Gt(ROSA)26Sortm4(ACTB-tdTomato,-EGFP)Luo/J (C57BL/6J-tdTomato), and C57BL/6J-*Tmem173*^{gt}/J (STING$^{\Delta}$) mice were obtained from Charles River Japan or The Jackson Laboratory. C57BL/6-Tg(TcraTcrb)1100Mjb/J (OT-I) mice were obtained from The Jackson Laboratory. C57BL/6-Ly5.1 mice (RBCC00144) were provided by the RIKEN BRC through the National BioResource Project of the MEXT/AMED, Japan. Mice were maintained and handled in accordance with the animal facility at Asahikawa Medical University or Hokkaido University.

Therapeutic studies in a mouse model

E0771 (2×10^5) or 3LL (3×10^5) cells were injected into the mammary fat pad or the right flank of mice, respectively. On day 7 after tumor implantation, tumor-bearing mice received intratumoral administration of PBS, anti-CD47 mAb (MIAP301, 5 µg in 25 µl of PBS/mouse; Bio X Cell), cGAMP (0.5 µg in 25 µl of PBS/mouse; Invivogen), or a combination of anti-CD47 mAb with cGAMP. Tumor mass was determined by measuring the tumor diameter at each indicated time point. Mice with tumors >300 mm^2 and 150 mm^2 were sacrificed in single-tumor and two-tumor models, respectively. For T cell depletion, 100 µg anti-CD8 mAb (53–6.72; Bio X Cell) or anti-CD4 mAb (GK1.5; Bio X Cell) was i.p. injected on days 6, 13, and 20 after tumor implantation. For blocking experiments, 100 µg anti-IFNAR1 mAb (MAR1-5A3; Bio X Cell) or anti-CXCR3 mAb (CXCR3-173; BioLegend) was i.p. injected on days 7 and 14 after tumor implantation. Rat IgG2a mAb (2A3; Bio X Cell), mouse IgG1 (MOPC-21; Bio X Cell), and hamster IgG mAb (HTK888; BioLegend) were used as isotype controls. For chemokine signal blocking analysis, 100 µg inhibitors for CCR2 (iCCR2; RS50493; Abcam) or CCR5 (iCCR5; maraviroc; Selleck) was i.p. administered to tumor-bearing mice 2 h before the mice received the intratumoral treatment. For addressing migration of monocytes/macrophages and T cells in a tumor site, tumor tissues were collected after 24 and 48 h of the treatments, respectively. To evaluate activation status of T cells in LNs, they were collected after 24 h of intratumoral treatment with each therapy. To evaluate tumor antigen-specific T cell responses, CD45.1$^+$OT-I cells were labeled with CFSE (Thermo Fisher Scientific) according to the manufacturer's instructions and transferred into E0771-OVA–bearing mice on day 7 after tumor inoculation, followed by intratumoral treatments. 4 d later, LNs and spleens were collected to assess OT-I cell responses by flow cytometry. All protocols were approved by the Asahikawa Medical University Institutional Animal Care and Use Committee or the Animal Ethics Committee of Hokkaido University.

Quantitative real-time PCR

Total RNA was purified from untreated mouse cell lines (E0771, 3LL, and MC-38) or the tumor tissues after 2 h (single-tumor model) or 6 h (two-tumor model) of treatment with intratumoral injection of anti-CD47 mAb and/or cGAMP using an RNeasy Micro Kit (Qiagen), reverse-transcribed by a PrimeScript first-strand cDNA synthesis kit (Takara Bio), and then amplified with LightCycler 480 Probes Master (Roche Life Science) and each probe according to the manufacturer's instructions. The following probes were obtained from Applied Biosystems (Life Technologies): *Mb21d1* (Mm01147496_m1), *Tmem173* (Mm01158117_m1), *Cxcl2* (Mm00441242_m1), *Ccl3* (Mm00441259_g1), *Ccl4* (Mm00443111_m1), *Ccl5* (Mm01302427_m1), *Ccl22* (Mm00436439_m1), *Cxcl9* (Mm00434946_m1), *Cxcl10* (Mm00445235_m1), *Cxcl11* (Mm00444662_m1), *Ifnb1* (Mm00439552_s1), *Mx1* (Mm00487796_m1), *Ova1* (Gg03366807_m1), and *Gapdh* (Mm99999915_g1). *Gapdh* was used as an internal control and to normalize each mRNA expression level. Relative expression levels were calculated in each experiment using the $\Delta\Delta C_t$ method.

Immunoblotting

Cells were lysed in RIPA buffer containing cOmplete Mini protease inhibitor cocktail (Roche). Whole-cell lysates were heated to 70°C in NuPAGE LDS sample buffer (Invitrogen) with 100 mM

dithiothreitol for 10 min, electrophoresed in 4–12% NuPAGE Bis-Tris SDS-PAGE gels (Invitrogen), and transferred to nitrocellulose membranes (Cytiva) using Power Blotter (Invitrogen). The membranes were blocked with 5% nonfat dry milk and incubated with primary antibodies overnight at 4°C followed by appropriate secondary antibodies. The following antibodies were purchased from Cell Signaling Technology: cGAS rabbit mAb (#31659), STING rabbit mAb (#13647), and anti-rabbit IgG, HRP-linked antibody (#7074). β-Actin (sc-47778; Santa Cruz Biotechnology) was used as a loading control. Anti-mouse IgG, HRP-linked antibody (NA931) was purchased from Cytiva. The reactive bands were visualized using chemiluminescence system (ECL Prime; Cytiva) and detected by iBright CL750 (Invitrogen). Relative expression levels were analyzed using iBright analysis software version 4.0.0 (Invitrogen).

Generation of BM chimeras

WT and STING$^{\Delta}$ mice were lethally γ-irradiated with 9.5 Gy (Gammacell 40; Nordion). After 24 h, mice were injected i.v. with 5 × 10^6 donor BM cells derived from WT or STING$^{\Delta}$ mice. After 8 wk, the BM-chimeric mice were inoculated with E0771 in the mammary fat pad. Migration of monocytes/macrophages in tumors treated with control or cGAMP was assessed after 24 h.

In vitro analysis using BMDMs

For generating BMDMs, lineage cells were purified from the BM of mice using a MACS magnetic cell isolation system (Miltenyi Biotec) and cultured in the presence of 20 ng/ml recombinant M-CSF (PeproTech). 7 d later, attached cells were collected and used as BMDM. For phagocytosis analysis, BMDMs were cocultured with E0771 cells, which were labeled with CFSE, in the presence of 10 μg/ml anti-CD47 mAb and/or 10 μg/ml cGAMP. 4 h later, cells were washed with PBS, stained with anti-CD11b mAb, and assessed for phagocytosis using a BD Accuri C6 Plus Flow Cytometer (BD Biosciences). For cell surface analysis, BMDMs were cocultured with unlabeled E0771 cells in the presence of 10 μg/ml anti-CD47 mAb and/or 10 μg/ml cGAMP. In some experiments, 10 μg/ml anti-IFNAR1 mAb (MAR1-5A3; Bio X Cell) was added in the culture. 24 h later, cells were washed with PBS and assessed for their cell surface molecules using a CytoFlex Flow Cytometer (Beckman Coulter).

Cell surface analysis

E0771 and 3LL cells were stimulated with control, rIFN-β (2,000 U/ml; BioLegend), or rIFN-γ (10 ng/ml; PeproTech) for 48 h and stained with anti-CD47 (miap301; BioLegend), anti-H-2K^b (AF6-88.5; BioLegend), and anti-PD-L1 (10F.9G2, BioLegend) or rat IgG2a,κ (RTK2758; BioLegend) and mouse IgG2a,κ (MOPC-173; BioLegend) isotype control antibody. Tumor-bearing mice received each treatment on day 7 after tumor implantation, and tumor tissues were collected after 24–48 h. For isolation of TILs, single-cell suspensions from tumor tissues were prepared using the Tumor Dissociation Kit (Miltenyi Biotec) and the gentleMACS dissociator (Miltenyi Biotec) according to the manufacturer's protocol. Cells were stained with anti-CD45 (I3/2.3), anti-CD11b (M1/70), anti-Ly6C (HK1.4), anti-Ly6G (IA8), anti-I-A^b (AF6-120.1), anti-CD24 (M1/69), anti-CD103 (2E7), anti-H-2K^b (AF6-88.5), anti-PD-L1 (10F.9G2), anti-CD80 (16-10A1), anti-CD86 (PO3), anti-CCR2 (SA203G11), anti-CCR5 (HM-CCR5), anti-CXCR3 (CXCR3-173), anti-LFA-1 (H155-78), anti-CD29 (HMβ1-1), anti-CD49d (R1-2), anti-CD3 (17A2), anti-CD4 (RM4-5), anti-CD8α (53–6.7), anti-CD69 (H1.2F3), anti-CD25 (PC61), anti-PD-1 (29F.1A12), anti-CD45.1 (A20), anti-IFN-γ (XMG1.2), or isotype control antibodies following treatment with anti-mouse CD16/32 mAb (93). The antibodies were purchased from BioLegend and conjugated with any one of the following: FITC, phycoerythrin, phycoerythrin combined with a cyanine dye (PE-Cy7), or allophycocyanin. Stained cells were analyzed using the BD Accuri C6 Plus cytometer and system software (BD Biosciences).

Intracellular cytokine analyses

To evaluate peptide-specific OT-I cell responses, lymphocytes were cultured with or without 10 μg/ml OT-I peptide (SIINFEKL; Genscript) in the presence of monensin solution (BioLegend). 6 h later, cells were washed with PBS; stained with anti-CD3 (17A2), anti-CD8α (53–6.7), anti-CD4 (RM4-5), or anti-CD45.1 (A20) mAbs for 15 min; fixed/permeabilized using the BD Cytofix/Cytoperm kit (BD Biosciences) for 20 min; and then stained with anti-IFN-γ mAb (XMG1.2) for 30 min. All antibodies were obtained from BioLegend. The stained cells were analyzed using a CytoFlex Flow Cytometer (Beckman Coulter).

ELISpot assay

For purification of CD11b$^+$Ly6C$^+$ monocytes/macrophages from tumor tissues, single-cell suspensions from tumor tissues were prepared after 24 h of intratumoral treatment with control, anti-CD47 mAb, cGAMP, or a combination. CD45$^+$ cells were isolated from the single-cell suspensions using the MACS isolation system (Miltenyi Biotech) according to the manufacturer's protocol, and then CD45$^+$CD11b$^+$Ly6C$^+$Ly6G$^-$ monocytes/macrophages were sorted using FACSAria II (BD Biosciences). The sorted monocytes/macrophages were cocultured with OT-I cells in a MAHAS4510 plate (Millipore) for 24 h. IFN-γ–producing T cell numbers were visualized by anti-mouse IFN-γ enzyme-linked immunospot assay (ELISpot, catalog no. 3321-2A; Mabtech) according to the manufacturer's protocol. BCIP/NBT plus substrate (Mabtech) was used for detection. Plates were scanned with an automated ELISpot plate reader (Autoimmun Diagnostika). Spots were counted and analyzed using the AID ELISpot plate reader software (Autoimmun Diagnostika).

ELISA

Lymphocytes were collected from treated (left) and untreated (right) TDLNs from mice after 24 h of intratumoral treatment with control, cGAMP, or the combination and separated into CD4$^+$ and CD8$^+$ T cells using the MACS isolation system (Miltenyi Biotech). These cells were cocultured with B16F10 and E0771 for 24 h. Production levels of IFN-γ in culture supernatants were measured by ELISA (BD Biosciences).

Statistical analysis

Statistical analysis was performed using GraphPad Prism 9.1.2 (GraphPad Software). The χ^2 test was used to compare the

correlation between the levels of CD47 expression, clinicopathological parameters, and immunological indicators. Kaplan–Meier survival curves were assessed by the log-rank (Mantel–Cox) test. Differences between two groups and among multiple groups were analyzed by using unpaired *t* tests and ANOVA (one-way or two-way) with Tukey's multiple comparison test, respectively. Data are presented as mean ± SD or SE, and $P < 0.05$ was considered statistically significant.

Online supplemental material

Fig. S1 shows a gating strategy for FACS analysis, individual tumor size of tumor-bearing mice, and cGAS and STING expression in mouse cell lines. Fig. S2 shows the expression of chemokines and their receptors in tumor tissues and expression levels of H-2K^b, CD80 and CD86 on WT- and STING$^{\Delta}$-derived BMDMs cocultured with E0771 in the presence of anti-CD47 mAb and/or rIFN-β1. Fig. S3 shows the independency of CD4$^+$ cells in the combination therapy and total number of CD4$^+$, CD4$^+$CD69$^+$, CD8$^+$, and CD8$^+$CD69$^+$ T cells in TDLNs and CLNs. Fig. S4 shows individual tumor size and the expression of chemokines and *Ifnb1* in a two-tumor mouse model; it also shows systemic tumor-specific T cell activation by the combination therapy.

Acknowledgments

We thank Rie Matsumoto (Department of Pathology, Asahikawa Medical University) for administrative assistance. This project used Asahikawa Medical University shared resources (Central Laboratory for Research and Education).

This work was supported by Japan Society for the Promotion of Science KAKENHI grant JP17K15633 (to K. Ishibashi), the Akiyama Life Science Foundation (grant to T. Ohkuri), and the Suhara Memorial Foundation (grant to T. Ohkuri) and was partially supported by the Joint Research Program of the Institute for Genetic Medicine, Hokkaido University (H. Kitamura).

Author contributions: T. Ohkuri and H. Kobayashi designed the study. A. Kosaka, K. Ishibashi, T. Nagato, H. Kitamura, Y. Fujiwara, and T. Ohkuri performed the experiments and analyzed the data. A. Kosaka and T. Ohkuri wrote the manuscript. All authors discussed the experimental data and approved the manuscript.

Disclosures: T. Ohkuri reported personal fees and non-financial support from Chugai Pharmaceutical Co., Ltd. outside the submitted work. No other disclosures were reported.

Submitted: 27 April 2020
Revised: 13 July 2021
Accepted: 3 September 2021

References

Alspach, E., D.M. Lussier, A.P. Miceli, I. Kizhvatov, M. DuPage, A.M. Luoma, W. Meng, C.F. Lichti, E. Esaulova, A.N. Vomund, et al. 2019. MHC-II neoantigens shape tumour immunity and response to immunotherapy. *Nature.* 574:696–701. https://doi.org/10.1038/s41586-019-1671-8

Baccelli, I., A. Stenzinger, V. Vogel, B.M. Pfitzner, C. Klein, M. Wallwiener, M. Scharpff, M. Saini, T. Holland-Letz, H.P. Sinn, et al. 2014. Co-expression of MET and CD47 is a novel prognosticator for survival of luminal breast cancer patients. *Oncotarget.* 5:8147–8160. https://doi.org/10.18632/oncotarget.2385

Baird, J.R., D. Friedman, B. Cottam, T.W. Dubensky Jr., D.B. Kanne, S. Bambina, K. Bahjat, M.R. Crittenden, and M.J. Gough. 2016. Radiotherapy Combined with Novel STING-Targeting Oligonucleotides Results in Regression of Established Tumors. *Cancer Res.* 76:50–61. https://doi.org/10.1158/0008-5472.CAN-14-3619

Bakst, R.L., H. Xiong, C.H. Chen, S. Deborde, A. Lyubchik, Y. Zhou, S. He, W. McNamara, S.Y. Lee, O.C. Olson, et al. 2017. Inflammatory Monocytes Promote Perineural Invasion via CCL2-Mediated Recruitment and Cathepsin B Expression. *Cancer Res.* 77:6400–6414. https://doi.org/10.1158/0008-5472.CAN-17-1612

Betancur, P.A., B.J. Abraham, Y.Y. Yiu, S.B. Willingham, F. Khameneh, M. Zarnegar, A.H. Kuo, K. McKenna, Y. Kojima, N.J. Leeper, et al. 2017. A CD47-associated super-enhancer links pro-inflammatory signalling to CD47 upregulation in breast cancer. *Nat. Commun.* 8:14802. https://doi.org/10.1038/ncomms14802

Chao, M.P., A.A. Alizadeh, C. Tang, J.H. Myklebust, B. Varghese, S. Gill, M. Jan, A.C. Cha, C.K. Chan, B.T. Tan, et al. 2010. Anti-CD47 antibody synergizes with rituximab to promote phagocytosis and eradicate non-Hodgkin lymphoma. *Cell.* 142:699–713. https://doi.org/10.1016/j.cell.2010.07.044

Chen, J., D.X. Zheng, X.J. Yu, H.W. Sun, Y.T. Xu, Y.J. Zhang, and J. Xu. 2019. Macrophages induce CD47 upregulation via IL-6 and correlate with poor survival in hepatocellular carcinoma patients. *OncoImmunology.* 8:e1652540. https://doi.org/10.1080/2162402X.2019.1652540

Cook, K.L., and D.R. Soto-Pantoja. 2017. "UPRegulation" of CD47 by the endoplasmic reticulum stress pathway controls anti-tumor immune responses. *Biomark. Res.* 5:26. https://doi.org/10.1186/s40364-017-0105-8

Corrales, L., L.H. Glickman, S.M. McWhirter, D.B. Kanne, K.E. Sivick, G.E. Katibah, S.R. Woo, E. Lemmens, T. Banda, J.J. Leong, et al. 2015. Direct Activation of STING in the Tumor Microenvironment Leads to Potent and Systemic Tumor Regression and Immunity. *Cell Rep.* 11:1018–1030. https://doi.org/10.1016/j.celrep.2015.04.031

de Silva, S., G. Fromm, C.W. Shuptrine, K. Johannes, A. Patel, K.J. Yoo, K. Huang, and T.H. Schreiber. 2020. CD40 Enhances Type I Interferon Responses Downstream of CD47 Blockade, Bridging Innate and Adaptive Immunity. *Cancer Immunol. Res.* 8:230–245. https://doi.org/10.1158/2326-6066.CIR-19-0493

Demaria, O., A. De Gassart, S. Coso, N. Gestermann, J. Di Domizio, L. Flatz, O. Gaide, O. Michielin, P. Hwu, T.V. Petrova, et al. 2015. STING activation of tumor endothelial cells initiates spontaneous and therapeutic antitumor immunity. *Proc. Natl. Acad. Sci. USA.* 112:15408–15413. https://doi.org/10.1073/pnas.1512832112

Diamond, M.S., M. Kinder, H. Matsushita, M. Mashayekhi, G.P. Dunn, J.M. Archambault, H. Lee, C.D. Arthur, J.M. White, U. Kalinke, et al. 2011. Type I interferon is selectively required by dendritic cells for immune rejection of tumors. *J. Exp. Med.* 208:1989–2003. https://doi.org/10.1084/jem.20101158

Foote, J.B., M. Kok, J.M. Leatherman, T.D. Armstrong, B.C. Marcinkowski, L.S. Ojalvo, D.B. Kanne, E.M. Jaffee, T.W. Dubensky Jr., and L.A. Emens. 2017. A STING Agonist Given with OX40 Receptor and PD-L1 Modulators Primes Immunity and Reduces Tumor Growth in Tolerized Mice. *Cancer Immunol. Res.* 5:468–479. https://doi.org/10.1158/2326-6066.CIR-16-0284

Fuertes, M.B., A.K. Kacha, J. Kline, S.R. Woo, D.M. Kranz, K.M. Murphy, and T.F. Gajewski. 2011. Host type I IFN signals are required for antitumor CD8+ T cell responses through CD8alpha+ dendritic cells. *J. Exp. Med.* 208:2005–2016. https://doi.org/10.1084/jem.20101159

Fuertes, M.B., S.R. Woo, B. Burnett, Y.X. Fu, and T.F. Gajewski. 2013. Type I interferon response and innate immune sensing of cancer. *Trends Immunol.* 34:67–73. https://doi.org/10.1016/j.it.2012.10.004

Gajewski, T.F., H. Schreiber, and Y.X. Fu. 2013. Innate and adaptive immune cells in the tumor microenvironment. *Nat. Immunol.* 14:1014–1022. https://doi.org/10.1038/ni.2703

Gautier, G., M. Humbert, F. Deauvieau, M. Scuiller, J. Hiscott, E.E. Bates, G. Trinchieri, C. Caux, and P. Garrone. 2005. A type I interferon autocrine-paracrine loop is involved in Toll-like receptor-induced interleukin-12p70 secretion by dendritic cells. *J. Exp. Med.* 201:1435–1446. https://doi.org/10.1084/jem.20041964

Grabowska, J., M.A. Lopez-Venegas, A.J. Affandi, and J.M.M. den Haan. 2018. CD169$^+$ Macrophages Capture and Dendritic Cells Instruct: The Interplay of the Gatekeeper and the General of the Immune System. *Front. Immunol.* 9:2472. https://doi.org/10.3389/fimmu.2018.02472

Harabuchi, S., A. Kosaka, Y. Yajima, M. Nagata, R. Hayashi, T. Kumai, K. Ohara, T. Nagato, K. Oikawa, M. Ohara, et al. 2020. Intratumoral STING activations overcome negative impact of cisplatin on antitumor immunity by inflaming tumor microenvironment in squamous cell carcinoma. *Biochem. Biophys. Res. Commun.* 522:408–414. https://doi.org/10.1016/j.bbrc.2019.11.107

Ishibashi, K., T. Kumai, T. Ohkuri, A. Kosaka, T. Nagato, Y. Hirata, K. Ohara, K. Oikawa, N. Aoki, N. Akiyama, et al. 2016. Epigenetic modification augments the immunogenicity of human leukocyte antigen G serving as a tumor antigen for T cell-based immunotherapy. *OncoImmunology.* 5: e1169356. https://doi.org/10.1080/2162402X.2016.1169356

Ishikawa, H., Z. Ma, and G.N. Barber. 2009. STING regulates intracellular DNA-mediated, type I interferon-dependent innate immunity. *Nature.* 461:788–792. https://doi.org/10.1038/nature08476

Kieper, W.C., M. Prlic, C.S. Schmidt, M.F. Mescher, and S.C. Jameson. 2001. Il-12 enhances CD8 T cell homeostatic expansion. *J. Immunol.* 166: 5515–5521. https://doi.org/10.4049/jimmunol.166.9.5515

Liu, X., Y. Pu, K. Cron, L. Deng, J. Kline, W.A. Frazier, H. Xu, H. Peng, Y.X. Fu, and M.M. Xu. 2015. CD47 blockade triggers T cell-mediated destruction of immunogenic tumors. *Nat. Med.* 21:1209–1215. https://doi.org/10.1038/nm.3931

Lo, J., E.Y. Lau, R.H. Ching, B.Y. Cheng, M.K. Ma, I.O. Ng, and T.K. Lee. 2015. Nuclear factor kappa B-mediated CD47 up-regulation promotes sorafenib resistance and its blockade synergizes the effect of sorafenib in hepatocellular carcinoma in mice. *Hepatology.* 62:534–545. https://doi.org/10.1002/hep.27859

Majeti, R., M.P. Chao, A.A. Alizadeh, W.W. Pang, S. Jaiswal, K.D. Gibbs Jr., N. van Rooijen, and I.L. Weissman. 2009. CD47 is an adverse prognostic factor and therapeutic antibody target on human acute myeloid leukemia stem cells. *Cell.* 138:286–299. https://doi.org/10.1016/j.cell.2009.05.045

Marcus, A., A.J. Mao, M. Lensink-Vasan, L. Wang, R.E. Vance, and D.H. Raulet. 2018. Tumor-Derived cGAMP Triggers a STING-Mediated Interferon Response in Non-tumor Cells to Activate the NK Cell Response. *Immunity.* 49:754–763.e4. https://doi.org/10.1016/j.immuni.2018.09.016

Murata, Y., Y. Saito, T. Kotani, and T. Matozaki. 2018. CD47-signal regulatory protein α signaling system and its application to cancer immunotherapy. *Cancer Sci.* 109:2349–2357. https://doi.org/10.1111/cas.13663

Nguyen, K.B., T.P. Salazar-Mather, M.Y. Dalod, J.B. Van Deusen, X.Q. Wei, F.Y. Liew, M.A. Caligiuri, J.E. Durbin, and C.A. Biron. 2002. Coordinated and distinct roles for IFN-alpha beta, IL-12, and IL-15 regulation of NK cell responses to viral infection. *J. Immunol.* 169:4279–4287. https://doi.org/10.4049/jimmunol.169.8.4279

Ohkuri, T., A. Ghosh, A. Kosaka, J. Zhu, M. Ikeura, M. David, S.C. Watkins, S.N. Sarkar, and H. Okada. 2014. STING contributes to antiglioma immunity via triggering type I IFN signals in the tumor microenvironment. *Cancer Immunol. Res.* 2:1199–1208. https://doi.org/10.1158/2326-6066.CIR-14-0099

Ohkuri, T., A. Kosaka, K. Ishibashi, T. Kumai, Y. Hirata, K. Ohara, T. Nagato, K. Oikawa, N. Aoki, Y. Harabuchi, et al. 2017. Intratumoral administration of cGAMP transiently accumulates potent macrophages for anti-tumor immunity at a mouse tumor site. *Cancer Immunol. Immunother.* 66:705–716. https://doi.org/10.1007/s00262-017-1975-1

Okazawa, H., S. Motegi, N. Ohyama, H. Ohnishi, T. Tomizawa, Y. Kaneko, P.A. Oldenborg, O. Ishikawa, and T. Matozaki. 2005. Negative regulation of phagocytosis in macrophages by the CD47-SHPS-1 system. *J. Immunol.* 174:2004–2011. https://doi.org/10.4049/jimmunol.174.4.2004

Oldenborg, P.A., A. Zheleznyak, Y.F. Fang, C.F. Lagenaur, H.D. Gresham, and F.P. Lindberg. 2000. Role of CD47 as a marker of self on red blood cells. *Science.* 288:2051–2054. https://doi.org/10.1126/science.288.5473.2051

Pan, Y., F. Lu, Q. Fei, X. Yu, P. Xiong, X. Yu, Y. Dang, Z. Hou, W. Lin, X. Lin, et al. 2019. Single-cell RNA sequencing reveals compartmental remodeling of tumor-infiltrating immune cells induced by anti-CD47 targeting in pancreatic cancer. *J. Hematol. Oncol.* 12:124. https://doi.org/10.1186/s13045-019-0822-6

Russ, A., A.B. Hua, W.R. Montfort, B. Rahman, I.B. Riaz, M.U. Khalid, J.S. Carew, S.T. Nawrocki, D. Persky, and F. Anwer. 2018. Blocking "don't eat me" signal of CD47-SIRPα in hematological malignancies, an in-depth review. *Blood Rev.* 32:480–489. https://doi.org/10.1016/j.blre.2018.04.005

Sallets, A., S. Robinson, A. Kardosh, and R. Levy. 2018. Enhancing immunotherapy of STING agonist for lymphoma in preclinical models. *Blood Adv.* 2:2230–2241. https://doi.org/10.1182/bloodadvances.2018020040

Sánchez-Paulete, A.R., Á. Teijeira, J.I. Quetglas, M.E. Rodríguez-Ruiz, Á. Sánchez-Arráez, S. Labiano, I. Etxeberria, A. Azpilikueta, E. Bolaños, M.C. Ballesteros-Briones, et al. 2018. Intratumoral Immunotherapy with XCL1 and sFlt3L Encoded in Recombinant Semliki Forest Virus-Derived Vectors Fosters Dendritic Cell-Mediated T-cell Cross-Priming. *Cancer Res.* 78:6643–6654. https://doi.org/10.1158/0008-5472.CAN-18-0933

Schadt, L., C. Sparano, N.A. Schweiger, K. Silina, V. Cecconi, G. Lucchiari, H. Yagita, E. Guggisberg, S. Saba, Z. Nascakova, et al. 2019. Cancer-Cell-Intrinsic cGAS Expression Mediates Tumor Immunogenicity. *Cell Rep.* 29:1236–1248.e7. https://doi.org/10.1016/j.celrep.2019.09.065

Shi, Y., W. Zheng, K. Yang, K.G. Harris, K. Ni, L. Xue, W. Lin, E.B. Chang, R.R. Weichselbaum, and Y.X. Fu. 2020. Intratumoral accumulation of gut microbiota facilitates CD47-based immunotherapy via STING signaling. *J. Exp. Med.* 217:e20192282. https://doi.org/10.1084/jem.20192282

Shuptrine, C.W., R. Ajina, E.J. Fertig, S.A. Jablonski, H. Kim Lyerly, Z.C. Hartman, and L.M. Weiner. 2017. An unbiased in vivo functional genomics screening approach in mice identifies novel tumor cell-based regulators of immune rejection. *Cancer Immunol. Immunother.* 66:1529–1544. https://doi.org/10.1007/s00262-017-2047-2

Sikic, B.I., N. Lakhani, A. Patnaik, S.A. Shah, S.R. Chandana, D. Rasco, A.D. Colevas, T. O'Rourke, S. Narayanan, K. Papadopoulos, et al. 2019. First-in-Human, First-in-Class Phase I Trial of the Anti-CD47 Antibody Hu5F9-G4 in Patients With Advanced Cancers. *J. Clin. Oncol.* 37:946–953. https://doi.org/10.1200/JCO.18.02018

Takashima, K., Y. Takeda, H. Oshiumi, H. Shime, M. Okabe, M. Ikawa, M. Matsumoto, and T. Seya. 2016. STING in tumor and host cells cooperatively work for NK cell-mediated tumor growth retardation. *Biochem. Biophys. Res. Commun.* 478:1764–1771. https://doi.org/10.1016/j.bbrc.2016.09.021

Vernon-Wilson, E.F., W.J. Kee, A.C. Willis, A.N. Barclay, D.L. Simmons, and M.H. Brown. 2000. CD47 is a ligand for rat macrophage membrane signal regulatory protein SIRP (OX41) and human SIRPalpha 1. *Eur. J. Immunol.* 30:2130–2137. https://doi.org/10.1002/1521-4141(2000)30:8<2130:aid-immu2130>3.0.co;2-8

Watkins-Schulz, R., P. Tiet, M.D. Gallovic, R.D. Junkins, C. Batty, E.M. Bachelder, K.M. Ainslie, and J.P.Y. Ting. 2019. A microparticle platform for STING-targeted immunotherapy enhances natural killer cell- and $CD8^+$ T cell-mediated anti-tumor immunity. *Biomaterials.* 205:94–105. https://doi.org/10.1016/j.biomaterials.2019.03.011

Willingham, S.B., J.P. Volkmer, A.J. Gentles, D. Sahoo, P. Dalerba, S.S. Mitra, J. Wang, H. Contreras-Trujillo, R. Martin, J.D. Cohen, et al. 2012. The CD47-signal regulatory protein alpha (SIRPa) interaction is a therapeutic target for human solid tumors. *Proc. Natl. Acad. Sci. USA.* 109: 6662–6667. https://doi.org/10.1073/pnas.1121623109

Wu, J., R. Zhang, G. Hu, H.H. Zhu, W.Q. Gao, and J. Xue. 2018. Carbon Monoxide Impairs $CD11b^+Ly\text{-}6C^{hi}$ Monocyte Migration from the Blood to Inflamed Pancreas via Inhibition of the CCL2/CCR2 Axis. *J. Immunol.* 200:2104–2114. https://doi.org/10.4049/jimmunol.1701169

Xu, M.M., Y. Pu, D. Han, Y. Shi, X. Cao, H. Liang, X. Chen, X.D. Li, L. Deng, Z.J. Chen, et al. 2017. Dendritic Cells but Not Macrophages Sense Tumor Mitochondrial DNA for Cross-priming through Signal Regulatory Protein α Signaling. *Immunity.* 47:363–373.e5. https://doi.org/10.1016/j.immuni.2017.07.016

Yu, P., Y. Lee, W. Liu, T. Krausz, A. Chong, H. Schreiber, and Y.X. Fu. 2005. Intratumor depletion of CD4+ cells unmasks tumor immunogenicity leading to the rejection of late-stage tumors. *J. Exp. Med.* 201:779–791. https://doi.org/10.1084/jem.20041684

Zhang, X., S. Sun, I. Hwang, D.F. Tough, and J. Sprent. 1998. Potent and selective stimulation of memory-phenotype CD8+ T cells in vivo by IL-15. *Immunity.* 8:591–599. https://doi.org/10.1016/S1074-7613(00)80564-6

Zhang, H., H. Lu, L. Xiang, J.W. Bullen, C. Zhang, D. Samanta, D.M. Gilkes, J. He, and G.L. Semenza. 2015. HIF-1 regulates CD47 expression in breast cancer cells to promote evasion of phagocytosis and maintenance of cancer stem cells. *Proc. Natl. Acad. Sci. USA.* 112:E6215–E6223. https://doi.org/10.1073/pnas.1520032112

Zhang, M., G. Hutter, S.A. Kahn, T.D. Azad, S. Gholamin, C.Y. Xu, J. Liu, A.S. Achrol, C. Richard, P. Sommerkamp, et al. 2016. Anti-CD47 Treatment Stimulates Phagocytosis of Glioblastoma by M1 and M2 Polarized Macrophages and Promotes M1 Polarized Macrophages In Vivo. *PLoS One.* 11:e0153550. https://doi.org/10.1371/journal.pone.0153550

Zhao, X.W., E.M. van Beek, K. Schornagel, H. Van der Maaden, M. Van Houdt, M.A. Otten, P. Finetti, M. Van Egmond, T. Matozaki, G. Kraal, et al. 2011. CD47-signal regulatory protein-α (SIRPα) interactions form a barrier for antibody-mediated tumor cell destruction. *Proc. Natl. Acad. Sci. USA.* 108:18342–18347. https://doi.org/10.1073/pnas.1106550108

Supplemental material

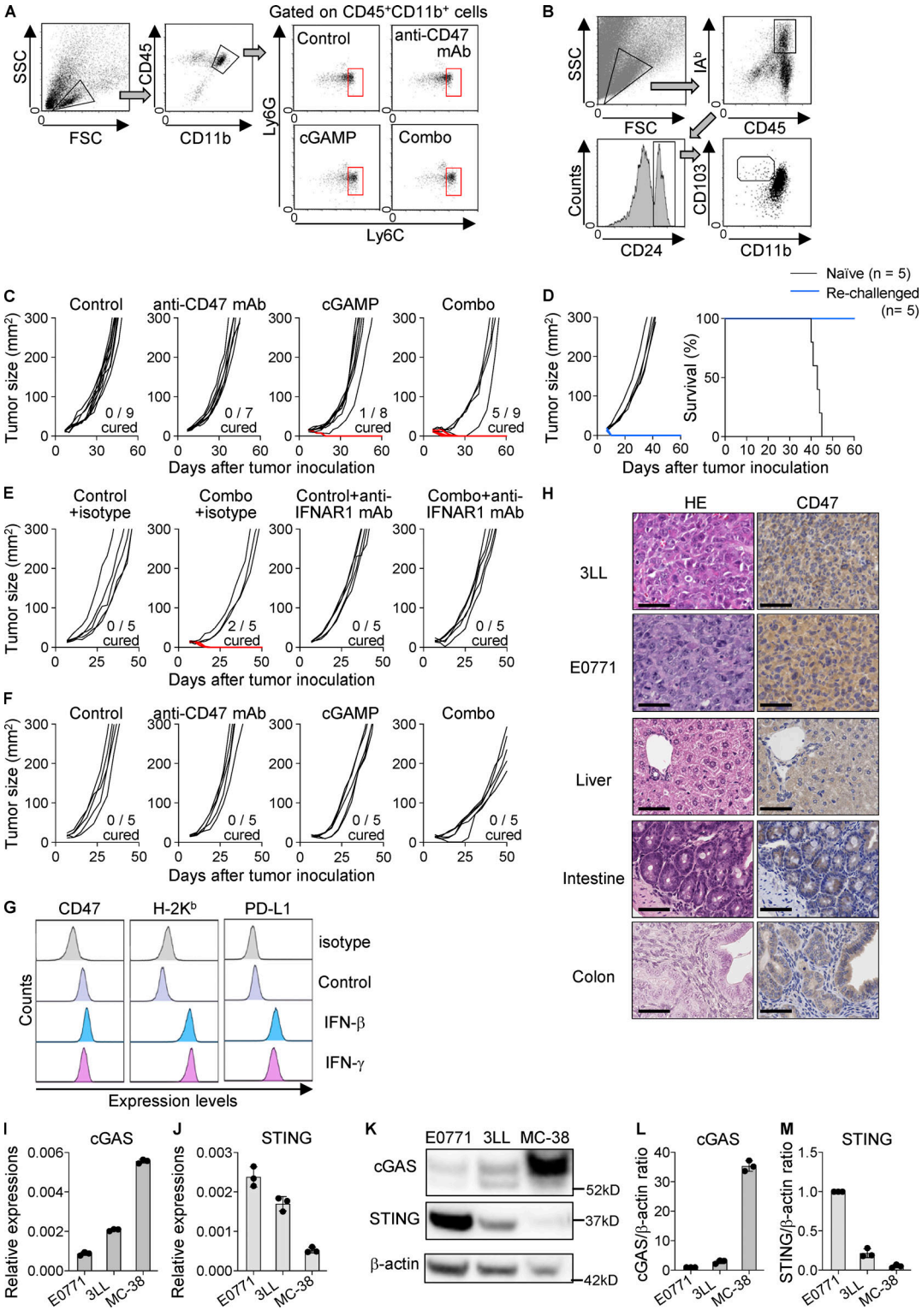

Figure S1. **Suppressed tumor growth and prolonged survival of mice receiving intratumoral coinjection of cGAMP and anti-CD47 mAb. (A and B)** Gating strategy for flow cytometry analysis of monocytes/macrophages ($CD45^+CD11b^+Ly6G^-Ly6C^+$; A) and cDC1 ($CD45^+I\text{-}A^{b+}CD24^+CD103^+CD11b^-$; B) in tumor tissues at 24 h after intratumoral treatment with anti-CD47 mAb and/or cGAMP. **(C–F)** Individual tumor sizes from Fig. 2 C (C), Fig. 2 G (E), and Fig. 2 I (F). The blue line represents completely rejected tumor growth. Completely cured mice by the combination therapy were rechallenged with E0771 cells (blue lines; $n = 5$). Naive mice were also inoculated with E0771 as a control (black lines; $n = 5$). Tumor size (left) and survival rates (right) were monitored (D). **(G)** Expression levels of CD47, H-$2K^b$, and PD-L1 of 3LL cells treated with rIFN-β (2000 U/ml) and rIFN-γ (10 ng/ml) for 48 h in vitro. Data are representative of two independent experiments. **(H)** Images of HE and CD47 staining in tumor tissues of 3LL and E0771, and normal mouse tissues of liver, intestine, and colon. Scale bars, 50 µm (images are representative of two samples). **(I–M)** cGAS and STING mRNA and protein expression in untreated cell lines ($n = 3$ for I, J, L, and M; $n = 1$ for K; data are representative of two independent experiments). Data are shown as mean ± SE.

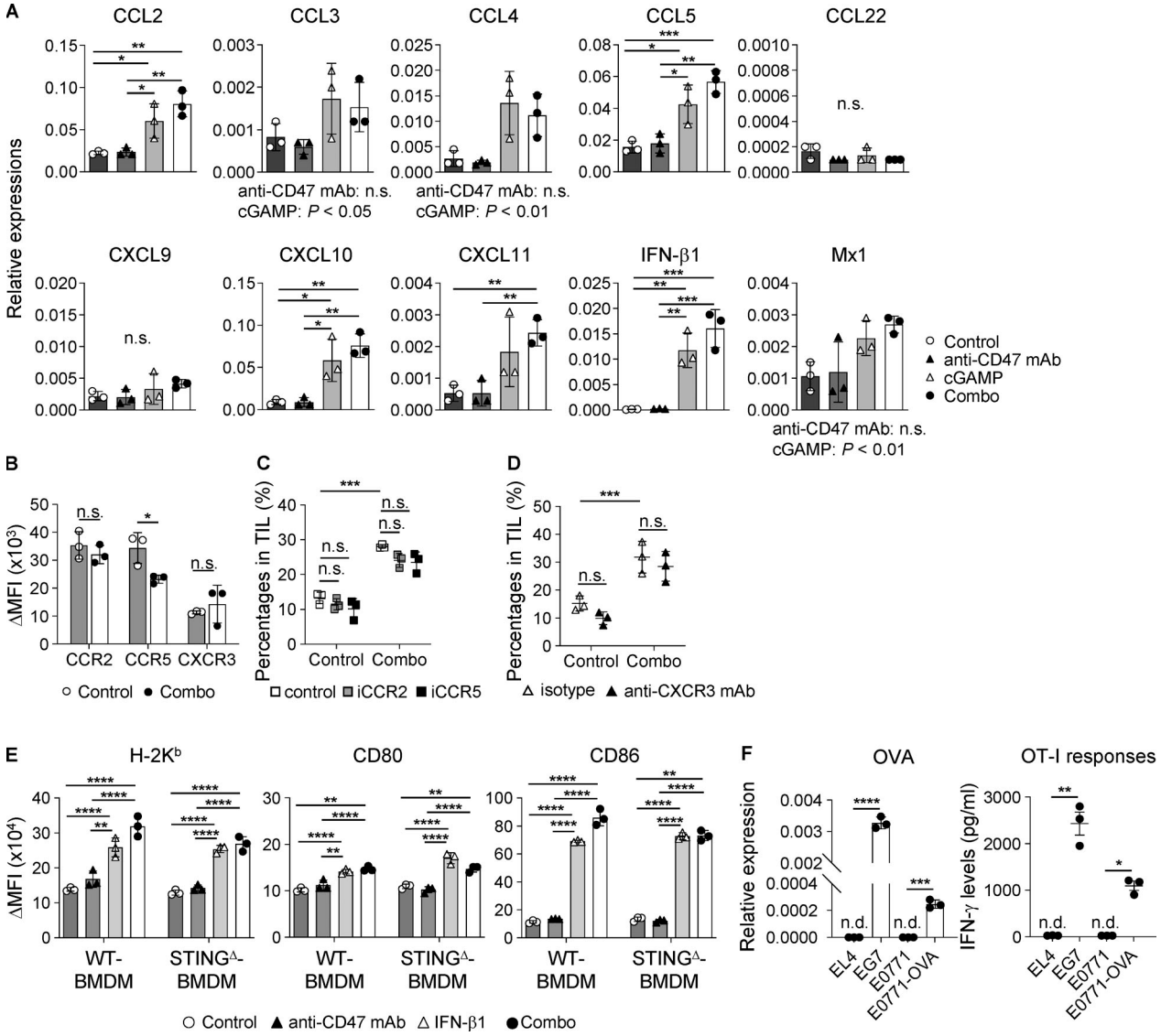

Figure S2. **Enhanced inflammatory responses by cGAMP-triggered type I IFNs. (A)** Gene expression levels in tumor tissues at 2 h after intratumoral treatment with anti-CD47 mAb and/or cGAMP (n = 3; data are representative of two independent experiments). **(B–D)** Monocytes/macrophages in TILs of WT mice were assessed at 24 h after intratumoral treatment with control and combination therapy with regard to expression levels of chemokine receptors (B) and for their percentages in the presence of inhibitors for CCR2 (iCCR2; 100 µg) or CCR5 (iCCR5; 100 µg; C) and blocking antibody for CXCR3 (anti-CXCR3 mAb; 100 µg; D), which were i.p. administered to mice 2 h before intratumoral treatment. Vehicle alone and isotype antibody were used as controls for the inhibitors and antagonistic antibody, respectively (n = 3; data are representative of two independent experiments). **(E)** Expression levels of H-2K^b, CD80, and CD86 on WT- and STING$^{\Delta}$-derived BMDM cocultured with E0771 in the presence of anti-CD47 mAb (10 µg/ml) and/or rIFN-β1 (2,000 U/ml) for 24 h (n = 3; data are representative of two independent experiments). **(F)** The OVA-encoding gene-transfected E0771 cell line (E0771-OVA) was established and validated by determining *Ova*l gene expression (left panel) and OT-I T cell responses (right panel) using real-time PCR and ELISA, respectively. Mouse EL4 and EG7 cell lines were used as negative and positive controls, respectively (n = 3; data are representative of two independent experiments). n.d., not detected. Change in (Δ)MFI against isotype control was calculated (target MFI minus control; B and E). Data are shown as mean ± SD (A–D) or SE (E and F). *, P < 0.05; **, P < 0.01; ***, P < 0.001; ****, P < 0.0001; two-way (A, D, and E) and one-way (C) ANOVA with Tukey's multiple comparison test and unpaired t test (B and F).

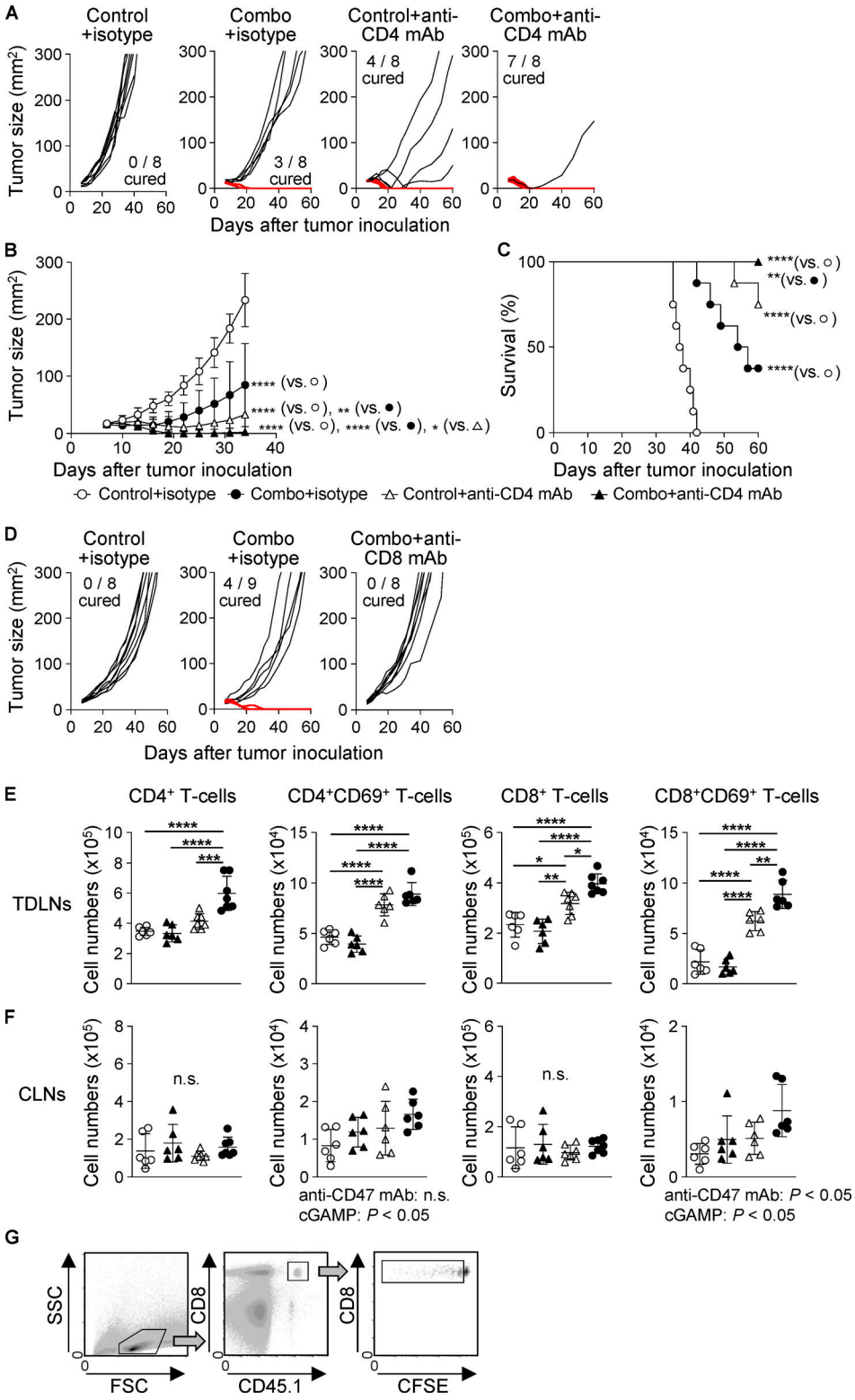

Figure S3. **CD8⁺ T cell–dependent efficacy of the combination treatment with cGAMP and anti-CD47 mAb.** E0771-bearing WT mice received intratumoral injection with control or combination treatment on day 7 after tumor implantation. **(A–D)** Isotype control antibody (100 µg), anti-CD4 mAb (100 µg; A-C), or anti-CD8 mAb (100 µg; D) was i.p. administered to WT mice on days 6, 13, and 20 after tumor implantation to deplete CD4⁺ or CD8⁺ T cells (n = 8–9 mice from two independent experiments). Tumor size (A, B, and D) and survival rates (C) were monitored. Mice with tumors >300 mm² were sacrificed. The red line represents complete tumor rejection. **(E and F)** Total numbers of CD4⁺, CD4⁺CD69⁺, CD8⁺, and CD8⁺CD69⁺ T cells in TDLNs (E) and CLNs (F) were assessed at 48 h after intratumoral treatments (n = 6; data represent two independent experiments). **(G)** Gating strategy for flow cytometry analysis of CFSE-labeled OT-I cells transferred into E0771-bearing mice. FSC, forward scatter; SSC, side scatter. Data are shown as mean ± SD. *, P < 0.05; **, P < 0.01; ***, P < 0.001; ****, P < 0.0001; two-way ANOVA with interaction followed by Tukey's multiple comparison test (B, E, and F) and log-rank (Mantel–Cox) test (C).

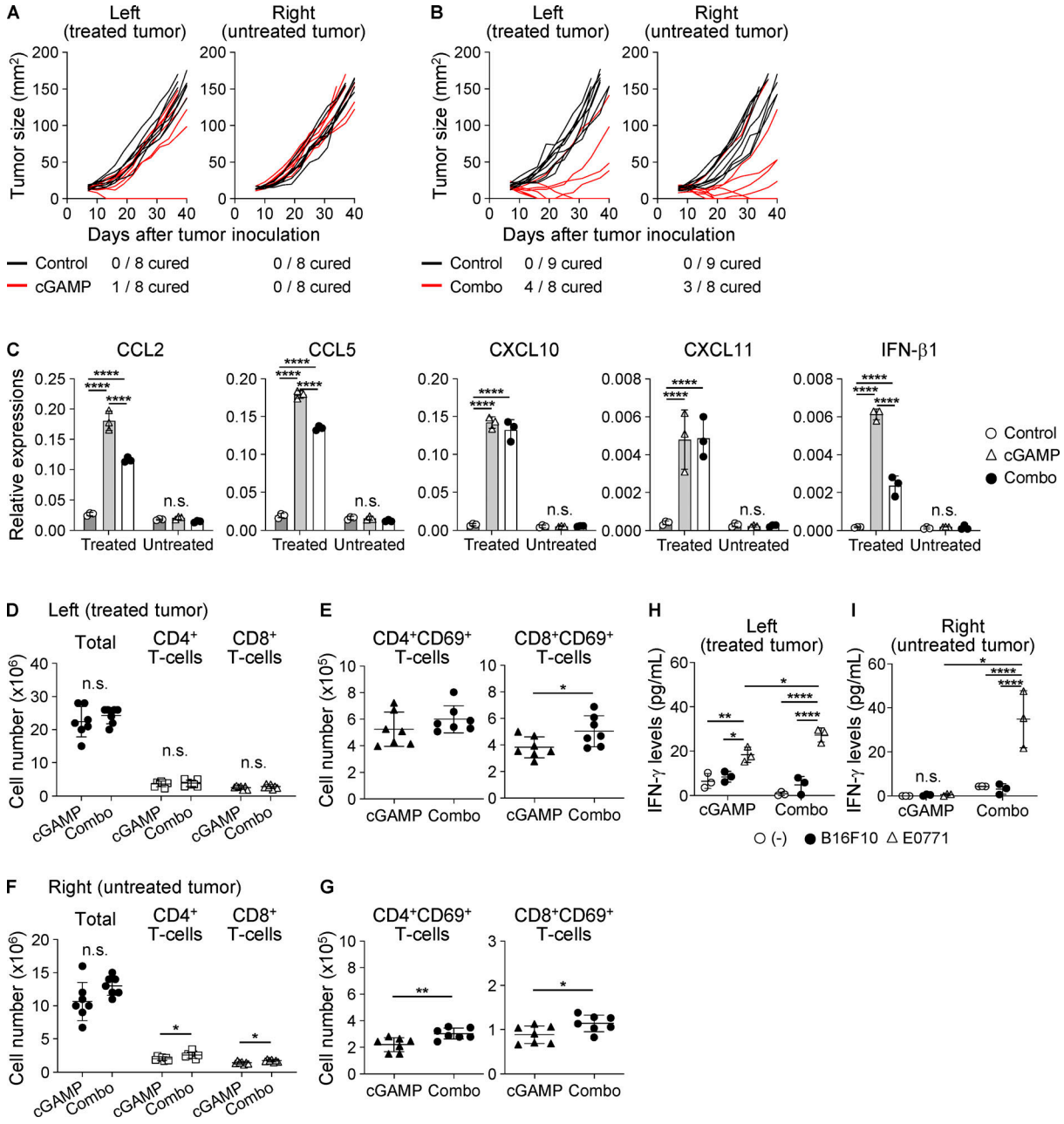

Figure S4. **Combination therapy with cGAMP and anti-CD47 mAb enhances systemic anti-tumor immunity.** WT mice were inoculated with E0771 cells in both left and right mammary fat pads and treated with control, cGAMP, or combination therapy in only the left tumor tissue on day 7. **(A and B)** Individual tumor sizes are shown (n = 8–9 mice from two independent experiments). Black and red lines represent tumor growth of mice treated with control and cGAMP (A) or combination (B) therapy, respectively. The number of cured mice is shown under the graph. **(C)** Gene expression levels in tumor tissues at 6 h after intratumoral treatment with anti-CD47 mAb and/or cGAMP (n = 3; data are representative of two independent experiments). **(D–I)** After 24 h of the intratumoral treatment, TDLNs were collected and assessed for the total numbers of $CD4^+$, $CD8^+$, $CD4^+CD69^+$, and $CD8^+CD69^+$ T cells in treated TDLNs (D and E) and untreated TDLNs (F and G; n = 7 mice from two independent experiments). The collected TDLN cells were cocultured with B16F10 or E0771 cells for 24 h. Production of IFN-γ from treated (left, H) and untreated (right, I) TDLN cells was assessed by ELISA (n = 3; data are representative of two independent experiments). Data are shown as mean ± SD. *, P < 0.05; **, P < 0.01; ****, P < 0.0001; one-way (C, H, and I) ANOVA with interaction followed by Tukey's multiple comparison test and unpaired t test (D–G).